Phonon-engineered extreme thermal conductivity materials

Phonon-Engineered Extreme Thermal Conductivity Materials

Xin Qian[1†], Jiawei Zhou[1†], and Gang Chen[1*]
[1]Department of Mechanical Engineering
Massachusetts Institute of Technology
Cambridge, MA 02139

[†]These authors contributed equally to this work.
*Corresponding email: gchen2@mit.edu

Abstract

Ultrahigh or low thermal conductivity materials are desirable for many technological applications such as thermal management of electronic and photonic devices, heat exchangers, energy converters, and thermal insulations. Recent advances in simulation tools (first principles, atomistic Green's function, and molecular dynamics) and experimental techniques (pump-probe techniques and microfabricated platforms) have led to new insights on phonon transport and scattering in materials, the discovery of new thermal materials, and are enabling the engineering of phonons towards desired thermal properties. We review recent advances in discovering both inorganic and organic materials with ultrahigh and low thermal conductivity, highlighting heat conduction physics, strategies, and future directions to achieve extreme thermal conductivities in solid-state materials.

Introduction

Thermal conductivity (k) characterizes the heat-conducting ability of materials, which spans from Xenon gas of 0.006 W/m-K to diamond of ~2000 W/m-K. Other than diamond, the next best-known heat conductor is SiC with k ~460 W/m-K. In the opposite direction, few materials have thermal conductivity between air (0.026 W/m-K) and polymers (~0.1 W/m-K). Discovering or engineering materials with ultra-high and ultra-low thermal conductivity is desirable for many applications such as thermal management of electronic and photonic devices, heat exchangers, and thermal insulations and energy converters. However, understanding and engineering of materials thermal conductivity has been a longstanding challenge in condensed matter and material physics, owing to the difficulty in modeling the many-body interactions among energy carriers, and the challenge in thermal measurements of samples with non-ideal shapes.

Heat in solids is mostly carried by electrons or atomic vibration. The electron contribution to thermal conductivity k_e is directly related to the electrical conductivity σ via the Wiedemann Franz law, $k_e = \sigma LT$, where L is the Lorentz number, which is a constant in metals and depends slightly on carrier concentration in semiconductors. The most electrically conductive material is silver, with also highest k in bulk metals (429 W/m-K).[1] For dielectric materials, the atomic vibration contributes to the majority of the thermal conductivity. Atomic vibrations in crystals are composed of normal modes, whose quanta are known as phonons. The vibration normal modes can be described by a dispersion relation $\omega(\boldsymbol{q}, s)$ with ω the phonon frequency as a function of $\boldsymbol{q}$ the wavevector and s the phonon polarization. Peierls described heat transport in dielectric

materials as motions and scatterings of phonons gas, using the Boltzmann transport equation (BTE).[2] This kinetic phonon gas model (PGM) laid the foundation for understanding heat conduction in crystals. For amorphous materials, normal modes still exist, but wavevectors are no longer well-defined due to the lack of periodicity. Allen and Feldman's theory[3] points out that vibrational modes in amorphous materials can be understood as propagons, diffusons, and locons. In Box 1, we summarized the thermal conductivity of crystalline and amorphous solids, and provided an overview of the physical picture of heat conduction.

Despite the early theoretical developments of heat conduction, [2-5] understanding the scattering dynamics of heat carriers remained phenomenological by fitting the simplified scattering models to the experimental data. The situation starts to change in the late 1990s, motivated by the need for thermal management of microdevices and thermoelectric energy conversion generation.[6,7] The Casimir regime, usually dominant at cryogenic temperatures, can become important at room temperature in thin films and nanostructures in microelectronic, optical, and optoelectronic devices. Because long MFP phonons are strongly scattered by the boundary, thermal conductivity becomes lower than bulk materials, which aggravates the concerns on the overheating problems in these devices.[6,7] On the other hand, the same effect can be explored to the benefit of thermoelectric energy conversion, for which materials with a low k but a high power factor.[8] These motivations have driven new developments in both computational and experimental tools for studying and engineering detailed scattering mechanisms of heat carriers. On the computational side, molecular dynamics (MD),[9,10] density functional theory (DFT),[11] and atomistic Green's function (AGF) [12] have liberated the field from the phenomenological fitting of experimental data. MD methods such as the nonequilibrium molecular dynamics (NEMD) and equilibrium molecular dynamics (EMD) provide an efficient way to gain atomistic level or phonon-modal level insights into heat conduction physics,[9,10] especially for complex systems such as disordered materials, alloys, polymers, and interfaces. The accuracy of MD method, however, has been limited by the empirical potential until the recent developments of Ab-initio MD methods[13] and machine learning potential fields[14] trained based on first-principles DFT data. On the other hand, the AGF method has been mostly applied to study interface conductances, and phonon-defect or phonon-nanoparticle scattering mechanisms. AGF has long been limited to harmonic/elastic scattering processes, until recent developments included anharmonic effects.[15] Particularly, the development of first-principles phonon simulation combining DFT and BTE has enabled predictions of thermal conductivity with high confidence, free of empirical parameters. In Box 2, we highlight the developments in first-principles methods, which enabled high fidelity prediction of thermal conductivity and provided scattering details across the entire phonon spectrum. On the experimental side, developments in thermal metrology also enabled characterizing the thermal transport process in ever-smaller spatial and temporal scales. In Box 3, we summarized the advances in experimental techniques for thermal conductivity measurement, as well as recent experimental developments in phonon MFP spectroscopy. [16,17]

These advances have led to new understandings in phonon scattering, and new strategies to minimize or maximize such scattering for extreme thermal conductivities. As shown in Fig. 1, different scattering strengths or MFPs including inelastic scattering such as phonon-phonon scattering and elastic scatterings such as phonon-defect scattering could result in different heat transfer regimes and various strategies for engineering thermal conductivity. Fourier diffusion regime is found when effective MFP $(1/\Lambda_{elastic} + 1/\Lambda_{inelastic})^{-1}$ is longer than wavelength λ but shorter than characteristic length d. In the diffusion regime, thermal conductivity can be tuned by

changing the scattering time through phonon band structure engineering. For example, ultrahigh thermal conductivity can be achieved via minimization of phonon-phonon scattering phase space and phonon-impurity scattering in bulk materials in the diffusion regime, which has been demonstrated in the discovery of cubic boron arsenide,[18-20] isotope enriched cubic boron nitride,[110] or in low dimensional structures, including polymer chains. Low k, on the other hand, can be achieved through multiple strategies, through intrinsically increasing anharmonicity or crystal complexity, or extrinsically introducing disorder, boundaries, interfaces and nanoparticles. In highly-disordered systems, Ioffe-Regel transition ($1/\Lambda_{elastic} + 1/\Lambda_{inelastic} \sim 1/\lambda$) might occur, and the thermal transport could be dominated by diffusons resulting glass-like low thermal conductivity.[21] Interfaces and boundaries can introduce size effects when the effective mean free path $(1/\Lambda_{elastic} + 1/\Lambda_{inelastic})^{-1}$ becomes longer than the sample (or heat source) size d, , which can also be used to tailor thermal conductivity. If the interface scatterings are phase destroying, classical size effect is expected with thermal conductivity lower than the bulk value, indicated by the Casimir-Knudsen regime in Fig.1. Interfaces and internal defects can be combined to scattering different spectral part of phonons, such as alloy composites with nanoparticles or grain boundaries with low k and superb thermoelectric performance.[22,23] On the other hand, if the interface scatterings are phase-preserving, coherence regime might be observed, such as passing bands in superlattices.[24,25] Interface scattering to the leading order is elastic, although inelastic scattering can also happen. Inelastic boundary scattering is part of the consideration on the phase destroying strength demarcating the coherent and Casimir-Knudsen regimes. One extreme of this coherent transport is the Anderson localization, when elastic scatterings inside the material are much stronger than inelastic scatterings ($\Lambda_{elastic}/\ \Lambda_{inelastic} << 1$) while inelastic scatterings are weak ($\Lambda_{inelastic}/\ d >> 1$), which might result in extremely low thermal conductivity. [26] The other extreme is the Fermi-Pasta-Ulam (FPU) regime in which case vibrations are not ergodic and phonon phases might be partially preserved, leading a divergent thermal conductivity despite the existence of inelastic scattering.[27] A special hydrodynamic regime might be expected when the normal scattering rate is the highest. Hydrodynamic thermal transport is usually observed when the characteristic size d (sample size or the period for transient grating experiment) is small enough, such that the boundary scattering dominates over Umklapp scattering, but weaker than normal scattering at the experimental temperature, namely $\gamma_{Normal} > v_g/d > \gamma_{Umklapp}$, where v_g is the group velocity of phonons. Hydrodynamic regime is potentially interesting for efficient heat spreading, since heat pulses could traveled as phonon population waves, known as the second sound.[28]

Due to these advances, it is timely to review recent progress on engineering phonon properties for thermal materials with ultra-high and low thermal conductivities. This review aims to summarize recent progress in both high and low thermal conductivity materials including both inorganic and organic ones with fundamental physical insights, and to inspire future research to push the boundaries of thermal materials.

Fig. 1. Transport regimes for heat conduction and engineering of thermal conductivity. The horizontal x-axis $\Lambda_{inelastic}/d$ is the MFP of inelastic phonon scattering inside bulk region (such as phonon-phonon interaction) normalized by the minimum characteristic size d (e.g. sample size for crystals, period for superlattices or size of heat sources for thermal transport measurements), and the vertical y-axis is the relative ratio of internal elastic MFP $\Lambda_{elastic}$ (such as phonon scatterings with isotopes, defects, alloys, inclusions and interfaces inside the material) to $\Lambda_{inelastic}$ (such as three-phonon and four-phonon processes). The third axis indicates other factors that commonly affect thermal transport, such as atomic mass and bulk modulus, and can be summarized by Slack's formula (Eq. 1). Along the horizontal axis, inelastic scattering strength decreases ($\Lambda_{inelastic}$ increases) and/or the sample size decreases, while along the vertical axis, the elastic scattering strength decreases and/or the inelastic scattering strength increases (the MFP ratio $\Lambda_{elastic}/\Lambda_{inelastic}$ increases). The arrows indicate the general directions to engineering extreme thermal conductivity materials: orange arrow with 'k↑' indicates direction to achieve high thermal conductivity, while blue arrows with 'k↓' indicate direction to achieve low thermal conductivity.

High thermal conductivity inorganic materials

High thermal conductivity (high-k) materials (>500 W/m-K) are desirable for heat dissipation in modern electronic devices. As shown in Fig. 2a, before the discovery of cubic boron arsenide (c-BAs) and boron nitride (c-BN), there existed no materials with thermal conductivity in the gap between 500 W/m-K and 2000 W/m-K. Slack proposed that thermal conductivity can be written as: [32]

$$k = A\frac{\bar{M}\delta\theta^3}{\gamma^2 T N^{2/3}} \quad (1)$$

where A is a proportional constant, N is the number of atoms in the unit cell, $\bar{M}$ is the mean atomic mass, with δ^3 is the average volume of each atom, θ is the Debye temperature and γ is the Grüneisen parameter. The Slack equation is valid for temperatures higher than Debye temperature θ. Since Debye temperature θ is proportional to the group velocity $v = \sqrt{B\delta^3/\bar{M}}$ where B is the bulk modulus, thermal conductivity scales with the mean atomic mass as $\bar{M}^{-1/2}$. Slack equation indicates that high k should be found in simple crystals consisting of lighter atoms and highly stiff bonds, and this equation still works well for a wide range of high-k materials, except for c-BAs as shown in Fig. 2b. Slack's theory predicted thermal conductivity of c-BAs is only ~ 200 W/m-K, and this material is overlooked for ~50 years as a potential candidate for ultrahigh k. Missing in the Slack theory are details in phonon scattering, which can be exploited to achieve higher thermal conductivity (Fig.1), as discussed below.

Figure 2. Discovery and bandstructure engineering of ultrahigh thermal conductivity materials. **a.** Bulk-materials with high thermal conductivity. The gap from 500 W/m-K to 2000 W/m-K is unfilled until the experimental demonstration of c-BAs (2018a.[18] 2018b[19] and 2018c[20]) and c-BN.[33] Theoretical predictions of BAs using Slack's equation,[34] three-phonon (3-ph) iterative solution of BTE[35], four-phonon (4-ph) using relaxation time approximation (RTA)[36] and iterative 4-ph.[19] This figure is modified from ref. [37]. Copyright by AAAS 2018. **b.** Thermal conductivity at room temperature versus the factor $\bar{M}\theta^3\delta$ in Slack equation, reproduced from ref.[38]. Copyright by Nature Publishing Group 2020. **c.** Large phonon bandgap of BAs suppresses three-phonon (3-ph) interaction, but four-phonon interaction is still allowed. This figure is reproduced from ref.[36] Copyright by American Physical Society 2017. **d.** Temperature dependent thermal conductivity[18-20] of BAs compared with c-BP,[39] diamond[19] and SiC[40].

Phonon band structure engineering The discovery of c-BAs in 2018 with ultrahigh k exceeding 1000 W/m-K is a manifestation of engineering phonon band structure by first-principles calculations[11]. Based on first-principles simulation, Lindsay and Broido[35] first predicted c-BAs potentially have thermal conductivity even higher than diamond at room temperature. This is because (1) acoustic phonon scatterings are weak due to the closely bundled longitudinal and transverse acoustic branches making energy and momentum conservations hard to satisfy, [41] and (2) acoustic-optical phonon scatterings are weak due to large phonon bandgap between optical and acoustic resulted from large mass difference between B and As atoms as shown in Fig 2c. Such detailed phonon scattering physics is missed in all past phenomenological models, and points to the direction of engineering phonon band structures for extreme thermal conductivity as shown in Fig.1. Although three-phonon interactions between acoustic and optical phonons are suppressed

by the large bandgap, energy conservation can still be satisfied if a fourth phonon is involved. Feng et al. discovered that indeed some four-phonon scattering processes are comparable to three-phonon scatterings in BAs, and including these higher-order interactions would reduce thermal conductivity to 1260 W/m-K,[36] which is still a very high thermal conductivity value.

These predictions have led to efforts by several groups to synthesize BAs and other boron-based materials, supported by a multidisciplinary university research initiative (MURI) program sponsored by the US Office of Naval Research. The synthesis of BAs was mainly done by chemical vapor transport, but the initial report of thermal conductivity in 2015 is only 200 W/m-K,[42] mainly due to the scattering of As vacancies, and values changed widely in different regions of the sample. Later, by selecting tiny BAs single crystals as seeds, and synthesis of BAs has progressed from tens of micron-sized samples to crystals of several millimeters in size. In 2018, several groups reported simultaneously thermal conductivity as high as 1200 W/m-K at room temperature using samples grown by three different groups,[18-20] summarized in Fig 2d. The samples typically have large spatial variations in thermal conductivity, and defect characterizations are still on-going.

Isotope enriched solids Natural crystals usually contain isotopes that introduce mass disorder that scatters phonons. Isotopically enriched crystals could have much enhanced thermal conductivity compared with the natural compounds. c-BN is an interesting example. First-principles simulation suggests that isotopically enriched c-BN can have a thermal conductivity as high as 2000W/m-K at room temperature.[43] Recently, ~90% enhancement of thermal conductivity of isotope enriched c-BN compared with natural c-BN is experimentally demonstrated. In fact, among the cubic boron-VI compounds (BN, BP and BAs), c-BN has the strongest isotope effect (Fig 2b). This is because as the boron-pnictogen mass ratio increases, the acoustic vibrations are becoming more dominant by the heavier pnictogen atoms which are naturally isotopically pure. Lindsay and Broido comprehensively studied the isotope effect using first-principles simulations,[43] and pointed out that large isotope effect is strongest in compounds with a large mass contrast ratio of elements and when the heavier atoms are isotopically enriched, such as GeC (448%) and BeSe (450%). However, GaN is discovered as a counterexample, with the predicted enhancement ~65% by isotope purification,[43] while later TDTR measurement of ^{71}GaN only found 15% enhancement at room temperature,[44] which is probably because higher-order phonon interactions are not considered in simulations yet.

Low-dimensional materials Low-dimensional structures such as carbon nanotube (CNTs) and graphene could have very limited scattering phase space, because certain scattering events are forbidden due to the selection rule protected by the crystalline symmetry.[45] For example in single-walled CNTs, selection rules dictate that Umklapp processes involving three acoustic phonon modes are not possible for single-walled CNTs.[46] Namely, Similarly, the mirror symmetry perpendicular to the basal planes of graphene forbids three phonon scattering events involving an odd number of out-of-plane ZA phonons. [47] As a result, thermal conductivity of CNT[48,49] and suspended graphene[50] are predicted higher than that of bulk graphite (2000 W/mK along the basal plane[51]). Low-dimension systems might even show diverging thermal conductivity[27,49]. Although CNTs are not exactly 1D systems like atomic-chain toy models, Mingo and Broido [52] pointed out that the thermal conductivity of CNTs diverges with the length L as L^n with the exponent n between 1/3 and 1/2, if only three-phonon processes are considered. Similarly, for 2D lattices, theory predicts that thermal conductivity of graphene diverges as $\log(L)$. [53] Experimental data

demonstrating the divergence of thermal conductivity of CNTs[54] or graphene[55] are scarce and have not proven divergence beyond doubt.

Low thermal conductivity inorganic materials

The interests in low thermal conductivity (low-k) materials stem from the need for thermal insulation. For typical thermal insulation purposes in applications like refrigerators, building materials, and windows, trapped gas such as argon used in windows is one best way other than the vacuum approach. However, some insulation applications require the materials to be dense solids. One example is thermoelectric materials that need to be electrically conducting but thermally insulating, which cannot be easily achieved via the porosity approach.[56] Another example is thermal barrier coatings at high temperatures. Although thermal barrier coatings have pores to suppress thermal expansion, lowering the thermal conductivity is still very important to suppress the undesired heat conduction for higher operating temperatures.[57] This section discusses the strategies that could be used for engineering thermal materials with low thermal conductivity, including strategies that lead to low thermal conductivity of the pristine materials. As shown in Fig 3a., intrinsic low k can be achieved via heavy elements, strong anharmonicity and complex unit cells. Whereas recent developments in first-principles provided new atomistic insights in the physical origins of giant anharmonicity. For complex crystals, recent studies have shown glass-like thermal transport can even be observed in complex crystals, due to the large population of diffuson-like modes.[58] Such Ioffe-Regel transition is also indicated in Fig. 1. Extrinsic methods are also discussed in this section. Due to the wide spectrum nature of thermal transport (Fig 3b), achieving extremely low thermal conductivity usually requires multi-scale structures such as embedding nanoparticles into alloyed nanocrystals or superlattices to scatter phonons across the wide frequency range in solids. For example, alloy scatterings suppress high-frequency phonon contribution, while nanoparticles and interfaces can scatter or even localize low-frequency phonons, as shown in the Anderson localization regime in Fig. 1.

Figure 3. Material design and engineering for ultralow thermal conductivity materials. a. Strategies for designing and screening for intrinsically low-k materials, including heavy elements (e.g. PbTe), strong anharmonicity through mechanisms like resonant bonding and so on, and complex unit cells (e.g. Clathrates). The middle panel is reproduced from ref [59,60], copyright by Nature Publishing Group 2014 and 2011, respectively. **b**. Schematic of spectral engineering to further suppress thermal conductivity. Full-spectrum suppression of thermal conductivity can be achieved by combining nanoparticles (NPs), superlattices (SLs), grain boundaries in nanocrystals (NCs) and alloying. The shading color indicates the part of spectral thermal conductivity that could be suppressed by including different structures. For example, if alloy/defect scatterings are included, the shaded blue area of intrinsic spectral thermal conductivity could be suppressed, and spectral thermal conductivity would shift to the boundary between the shaded green and blue regions. If we further including boundary scattering, NPs and SLs, the spectral thermal conductivity in the green region and yellow region could be suppressed, with only low-frequency phonons contributing to the thermal conductivity (shaded red region).

Strategies for intrinsically low thermal conductivity Opposite to high-k solids, low-k materials usually have heavy elements, weak interatomic bonds, strong anharmonicity, and complex unit cells (Fig. 3a) to ensure small group velocities and short relaxation times. Indeed, some of the best

thermoelectric materials including Bi_2Te_3 and PbTe are composed of heavy elements. However, understanding of anharmonicity was grouped into the Grüneisen parameter without providing details of phonon interaction dynamics. First-principles simulation provided new insights on the strategies to achieve giant anharmonicity. One example is the rattling modes usually found in caged systems such as clathrates[61] and skutterudites[62], which are low-lying vibrational branches due to the weak coupling of the host lattice with the heavier guest-filler atoms. These low-lying branches would strongly scatter acoustic phonon branches, resulting in low thermal conductivity. The ultralow thermal conductivity of Tl_3VSe_4 (0.3 W/m-K) is also found related to strong anharmonicities due to the weakly bounded Tl atoms behaving similarly to rattlers.[63] Later work by Xia et al pointed out that phonon renormalization and four-phonon scattering due to the fourth-order force constants are important to explain the experimental results.[64] Resonant bonding is another mechanism for achieving giant phonon anharmonicity and low thermal conductivity. Resonant bonding in PbTe is responsible for the highly delocalized electron distributions and soft transverse optical (TO) branches, resulting in strong acoustic and optical phonon interaction.[59,60] Without such interactions, the thermal conductivity of PbTe would be five times higher.[65] Resonant bonding is also shown responsible for the lattice instability of SnSe and its strong anharmonicity.[66] Finally, looking for low-k materials in complex crystals with large unit cells is also a fruitful direction, since the Slack equation suggests that thermal conductivity scales with the number of atoms (N) in unit cells as $N^{-2/3}$. Although amorphous materials usually have lower thermal conductivity than crystals due to the existence of diffusons and locons, applications like thermoelectrics require good electrical conductivity, and thermal barrier coatings requiring high-temperature stability, which are not easily achieved in amorphous materials. Recent studies[58] found that complex crystals could even exhibit glass-like thermal conductivity, since they simultaneously host propagons and diffusons, which cannot be well explained by PGM. For example, higher manganese silicate with nano-sized unit cell (a= 5.5 Å, c= 47.7 Å) is shown to have thermal conductivity lower than the k_{min} limit (Box 1), due to the predominance of diffuson modes.[58] Organic-inorganic hybrid crystals are another interesting type of complex crystals with ultralow thermal conductivity, because of the weak coupling between the organic ligands and inorganic frameworks, and the dynamical disorders due to internal degrees of freedom of organic ligands. For example, organometal halide perovskites showed ultralow thermal conductivity in the range of 0.3~0.5 W/m-K, [67-69] because of the soft bonds and the coexistence of phonons and diffusons.[70]

Alloys and Disordered Solids In addition to tailoring bonding anharmonicity, phonon scattering rates can also be enhanced by extrinsic methods through introducing disorders. Scattering with structural disorders would suppress the phonon MFP. Alloying, a common approach to introduce disorder first pioneered by Ioffe in the 1950s, [71] is almost exclusively used in thermoelectric materials to improve the thermoelectric figure of merit. The mass disorder is particularly effective in scattering high-frequency phonons, with scattering rates scales as $\tau^{-1} \sim \omega^4$ at low frequency limit, similar to Rayleigh scattering.[72] First-principles simulations based on virtual crystal approximation (VCA) and Tamura's perturbation theory for mass-disorder scattering have shown effective in reproducing experiments.[73] However, VCA could lead to the overestimated thermal conductivity of alloys such as $In_{1-x}Ga_xAs$ [73] and $PbTe_{1-x}Se_x$.[74] Recently, Mingo's group found that alloying could also result in inhomogeneity in the local force fields, and force-field inhomogeneity could be captured using the *T*-matrix method.[75] While atomic impurities effectively scatter high frequency, the atomic defects are unseen by low-frequency phonons, which still contribute to

thermal conductivity. To further effectively reduce the thermal conductivity of alloys, the concept of "nanoparticles-in-alloy" has been demonstrated, [22,23] where nanoparticles are introduced to further scatter the mid- to low-frequency phonons.

In contrast to simple crystals, anharmonicity could increase thermal conductivity for solids with a large number of non-propagating modes such as complex crystals and amorphous materials. Recent theory developed by Simoncelli et al., [76] and Isaeva et al.[77], showing that the overlap of vibrational modes with large linewidths at similar frequencies could contribute to thermal conductivity. Their theory includes the effect of anharmonicity and unified the PGM for crystals and Allen-Feldman theory for amorphous materials. This unified theory showed that thermal conductivity is composed of contributions from a phonon gas part (k_P) like propagons and a "coherent" term (k_C) which describes the quasi-degenerate transition of vibrational modes. At low temperature, k_C is dominated by the degenerate states with same frequency, which is the same as the Allen-Feldman theory, but at room temperature and higher temperature, k_C due to the tunneling between modes at different frequencies could become considerable, which is originated from anharmonicity and the resulting finite linewidths of vibrational branches.

Interface and Boundaries Reducing thermal conductivity via interface and boundaries in thin films, nanowires and nanocomposites is another major direction.[78] Although the classical size effect has been well known since the work of Casimir,[79] the interests become revitalized with concerns on thermal management in electronics and optoelectronic devices and thermoelectric materials. In nanostructures, thermal conductivity is usually lower than bulk crystals, due to the classical size effect (Fig. 4a-b). In such classical size regime, film thicknesses are usually comparable or smaller than phonon MFPs, and phonons are often scattered by the boundary. This effect has been effectively incorporated into the development of thermoelectric materials.[8,23] Some extraordinarily low thermal conductivity has been observed in van der Waals layered materials. Cahill's group discovered through-plane thermal conductivity in randomly stacked WSe_2[29] is twice of air at room temperature, much lower than the k_{min} model prediction. Similarly, Pop's group showed heterogeneous stacking of 2D materials can result in thermal conductivity lower than air.[30] Exact mechanisms of such extreme low thermal conductivity remain to be clarified.

One intriguing question is if one can exploit the wave nature of phonons to engineer thermal conductivity, as has been done for photons and electrons routinely. The challenges are that the major heat-carrying phonons are broadband (from ~100 GHz to ~10 THz), highly anharmonic, and usually have very short wavelengths. Superlattices are good test-ground for coherent phonon transport. If phonon scattering at individual interfaces ruins phonon phases, transport is in the classical Casimir regime.[80,81] If the phonons maintain their phases, namely inelastic phase-destroying scattering is much weaker than elastic scattering, transport is in the coherent regime, as shown in Fig. 1. Extensive studies show that the significantly lower thermal conductivities of superlattices are due to diffuse phonon scattering at interfaces caused by interfacial atomic mixing or other defects.[82] However, low frequency and long-wavelength phonons can still maintain their phase and remain coherent, when the superlattice period is smaller than inelastic phonon MFPs ($\Lambda_{inelastic}/d > 1$) and when the interface scattering is phase preserving. These coherent phonons form mini-bands and transport ballistically across the entire superlattice sample, so coherent phonon transport can be characterized by measuring thermal conductivity of [83]GaAs/AlAs superlattices as a function of the number of periods, which corresponds to the coherent regime shown in Fig. 1. In addition, phonon coherence[24,25] can also be effectively tuned by the interface density in

superlattices, i.e., changing the periodic thickness. In contrast to the incoherent regime, increasing the interface density would result in an increased thermal conductivity in the coherent regime (Fig. 4c), [25,84] because of wave tunneling,[85] although another possibility is that decreasing the period thickness makes the superlattices behavior like a bulk alloy due to interface mixing. Although coherent phonons extending through the superlattice have reduced group velocity due to mini-gaps,[86] they propagate through many interfaces and could have longer MFPs that overcome the reduced group velocity, leading to a thermal conductivity larger than the case of phonons being scattered incoherently at individual interfaces of the superlattices. With interface mixing scattering high-frequency phonons and reducing the thermal conductivity of superlattices, the persistent long-wavelength coherent phonons could contribute dominantly to heat conduction in superlattices, although their contribution is usually small for heat conduction in bulk materials.

The long-wavelength coherent phonons might be coherently scattered by nanoparticles of appropriate size. Interestingly, experiments in 3nm GaAs/3nm AlAs superlattices embedded with ErAs dots of ~3 nm in diameter at interfaces have shown signatures of Anderson localization at cryogenic temperatures (Fig. 4d-e). [26] In the Casimir-Knudsen regime, thermal conductivity would increase with the number of periods, i.e., the total thickness of samples, which are observed for smaller sample thicknesses. At cryogenic temperatures, as the sample thickness further increases, the thermal conductivity peaks with the number of periods and then decreases with an increasing number of periods, which is a signature of Anderson localization. At higher temperatures, however, phonon-phonon scattering becomes dominant due to anharmonicity and the phonon transport is no longer in the wave-regime, hence Anderson localization is destroyed (Fig. 4e). These recent developments on coherent heat conduction and localization are exciting as it illustrates the potential to engineer phonon heat conduction in the wave regime as people have achieved routinely for photons and electrons. There are also other studies suggesting phonon wave effects such as in phononic crystals with characteristic length >100 nm or larger at cryogenic temperatures.[83] However, it is unlikely that phonon wave effects can become appreciable in 100 nm structures. Retaining the coherence feature at room temperature is also a challenge due to the intrinsic phase-destroying inelastic phonon scatterings.

Figure 4. Phonon-Interface Interaction. **a-b** Thermal conductivity reduction in the incoherent regime. **a**. Thermal conductivity Si thin films by theoretical prediction[87] and experiments[87-90] and **b**. Silicon nanowires with symbols representing experiments by Li et al.[91] and lines theoretical prediction by Dames et al. [92] **c-e** Coherent phonon transport in superlattices. **c**. Cross-over from incoherent regime to the coherent regime in $SrTiO_3/CaTiO_3$ (STO/CTO) superlattices on $NdGaO_3$ (NGO), STO and LSAT (100) substrate. The solid line is the modified Simkin-Mahan (SM) model prediction.[25] This figure is reproduced from ref.[25], copyright by Nature Publishing Group 2014. **d**. SEM picture of GaAs/AlAs superlattice embedded with ErAs nanoparticles. [26] **e**. Measured thermal conductivity as a function of the total number of periods in the superlattice. The peak in thermal conductivity at 30 K and 50 K indicates Anderson Localization. [26] d and e are reproduced from ref. [26], copyright by AAAS 2016.

Organic materials

Polymers have drawn increasing attention with the potential for both ultrahigh and ultralow thermal conductivities. On one hand, polymer chains are mostly randomly coiled, and hence almost all polymers have low thermal conductivity between 0.1 – 0.5 W/m-K[93]. On the other hand, a straight individual polymer chain resembles a one-dimensional crystal, and theoretical studies inspired by the Fermi-Pasta-Ulam model have indicated that certain vibrational modes do not decay with time in low dimensional systems,[27] suggesting a polymer chain may even possess a divergent thermal conductivity (FPU divergence regime in Fig 1). First-principles prediction of divergence is shown in Fig. 5a. Despite these possibilities and various processing techniques available, recent work has just started to explore the upper and lower limit of the thermal transport in polymers.

Figure 5. **Heat conduction in organic materials**. **a**. Molecular dynamics simulation shows a single polyethylene chain can have a divergent thermal conductivity.[94] **b**. Phonon dispersion of polyethylene crystal from first-principles calculations. The inset shows the polyethylene crystalline structure. **c**. Cumulative thermal conductivity with phonon mean free path in polyethylene crystal from first-principles calculations.[95] **d.** Thermal conductivity with respect to the draw ratio from past experiments by Shen et al.[96] Xu et al. [97] Choy et al., [98], by Piraux et al.[99] Error bars are obtained from the original literatures if available. The inset illustrates the effect of drawing on crystalline domain orientation and chain alignment. **e**. Illustration of chain conformation transition, which facilitates heat transport along the chains. **f**. Repulsive forces from charged backbone at higher pH leads to an extended chain in a polyelectrolyte that enhances thermal conductivity, while the thermal conductivity of a neutral polymer is unchanged with pH.[100] **g**. Illustration of engineering intermolecular interactions, which favor inter-chain heat transfer. (h) Examples of intermolecular forces that have been engineered leading to enhanced thermal conductivity in polymers[101-103].

Semi-crystalline polymers Driven by the desire to achieve highly heat-conducting polymers, MD[94,104,105106] and first-principles simulations[95,107] have been used to investigate the heat conduction limit in polymer chains and polymer single crystals. Strong bonds (e.g. carbon double bonds) and rigid structures (e.g. aromatic backbone) generally facilitate heat conduction. In particular, Minnich et al. predicted a high thermal conductivity of 160 W/m-K at room temperature in crystalline polyethylene along the chains using first-principles calculations,[95] with major contributions from longitudinal acoustic phonons having MFPs from 10 nm to 1 μm. However, such perturbative methods cannot capture strong correlations as in the Fermi-Pasta-Ulam regime (Fig. 5b-c). Using MD simulations, Luo et al. showed that polyacetylene has an even higher thermal conductivity than polyethylene due to conjugated π bonds .[106] Polymers are at most semi-crystalline, with nanoscale crystalline domains embedded in an amorphous matrix.[93] Early efforts increased the thermal conductivity of polyethylene and polyacetylene (Fig. 5d) to 20 – 40 W/m-K, [108] through mechanically stretching the polymers. Recent efforts[96,109] have achieved thermal conductivity on mechanically stretched ultrahigh molecular weight polyethylene nanofibers over 100 W/m-K and polyethylene films over 60 W/m-K (Fig. 5d).[97] The polyethylene films synthesized using gel spinning followed by hot stretching are found to consist of self-assembled nanofibers due to the inter-chain van der Waals couplings.[97] Detailed structural characterizations

show that each individual fiber consists of alternate crystalline and amorphous segments, and thermal conductivity of amorphous region could even reach 16 W/m-K, showing the significance in engineering the amorphous domains. By electrodepositing amorphous polythiophene into a nanochannel template, thermal conductivity as high as ~4.4 W/m-K had been reported.[110] Different synthetic/processing approaches can also be used. By stretching catalytically disentangled polyethylene with a draw ratio over 200 times, Ronca *et al* achieved a thermal conductivity of 65 W/m-K.[111] Zhu *et al* subjected commercially available polyethylene microfiber to further heat-stretching, and reported thermal conductivity as high as 51 W/m-K.[112] Given that most work has been focused on polyethylene only, there is significant room to further increase the thermal conductivity in other polymers. [113,114]

Amorphous polymers Whereas axially stretched polymers have high thermal conductivity in one direction, isotropic heat-conducting polymers are easier to be made into composites and can broaden the scope of applications. [115] Amorphous polymers are intrinsically isotropic, but current understanding of their thermal transport is relatively poor owing to their disordered nature. MD simulation [116] is the primary means to uncover the correlation between thermal transport and their microscopic structure. Extended chain conformation with a large radius of gyration is found to faciliteate heat conduction along the chains[116] (Fig. 5e). Experimentally, an extended chain can be stabilized by favorable interactions between polymers and solvent and unfavorable interactions among polymers themselves.[93] Pipe *et al* utilized the repulsive Coulombic forces between charged groups on the backbone of polyelectrolytes to stretch out the polymer chains in a spin-cast film. The resulting extended chain conformation leads to an enhanced thermal conductivity up to ~1.2 W/m-K (Fig. 5f).[100]

Weak interactions between polymer chains are another dominant source of thermal resistance, and efforts have been geared towards engineering interchain interactions (Fig. 5g). [101,103,117] In an amorphous polymer, a stronger inter-chain interaction can facilitate heat conduction across different chains and enhance the thermal transport in the random polymer network. As a comparison, the bond energy of typical van der Waals interaction is less than 5 kJ/mol, while ionic and π-π interactions can have bond energy up to ~200 kJ/mol and ~50 kJ/mol, respectively. By characterizing the thermal conductivity of water-soluble polymers with different inter-chain interactions from ionic to hydrogen bonding, Cahill *et al* showed that the thermal conductivity varying from 0.14 W/m-K to 0.67 W/m-K generally increases with the mechanical stiffness and the sound velocity,[101] suggesting stronger inter-chain interactions facilitate heat conduction. Xu *et al.*[103] explored π-π stacking in poly(3-hexylthiophene) grown using an oxidative chemical vapor deposition approach and achieved an order of magnitude increase in the thermal conductivity. The π-π interactions not only contribute to the inter-chain interactions, but also lead to an ordered polymer structure at optimized processing temperature. Recent work also showed that by leveraging π-π interactions between monomers, epoxy resin can reach thermal conductivity close to 1 W/m-K,[102] opening up the prospect of developing heat-conducting polymer composite for thermal management applications (Fig. 5h).

Breaking the limit An open question is whether polymer chains can indeed possess divergent thermal conductivity corresponding to the FPU divergence regime in Fig. 1, both from theoretical and experimental standpoints. A non-perturbative approach is needed to study the divergence question, which may benefit from recent theoretical development in heat conduction rooted in many-body physics.[76,77] Experimentally, measurements on short polymer chains, in the form of arrays or individual chains, [118] show that thermal transport along chains is dominantly ballistic.[119]

However, these chains are less than 5 nm long and cannot answer questions on the divergence of heat conduction. Currently, there is significant gap between the microscopic dynamics and macroscopic thermal transport properties in polymers. Ample room exists in understanding the heat conduction mechanisms for further pushing their upper thermal conductivity limit.

The opposite direction, reducing the thermal conductivity of organic materials, remains largely unexplored. There are efforts exploring organic thermoelectric materials,[120] based on the fact that organic materials such as polymers already have low thermal conductivity. Concepts explored for achieving low k in inorganic materials can be applied to organic systems to further reduce their thermal conductivity. For example, dense fullerene-based organic compounds have been found to have thermal conductivity of 0.03 – 0.06 W/m-K (only slightly higher than that of air), [121] mainly due to the weak interactions between fullerenes. Alternatively, block polymers that resemble two-dimensional superlattices in inorganic materials may also possess low thermal conductivity if the periodic length scale is comparable or smaller than the MFPs of dominant heat carriers. In addition, disorder can be introduced into the polymer backbone through side chains or different tacticities. An interesting question is whether localization can be explored in polymers, as they intrinsically resemble one-dimensional systems. Combining organic and inorganic materials into composites, nanocrystals, or superlattices might also be an interesting direction for further reducing the thermal conductivity, due to the drastically mismatched vibrational spectra and their structural diversity. [122,123] For example, organic ligand stabilized inorganic nanocrystal arrays have shown thermal conductivity as low as 0.05 W/m-K recently.[124]

Future directions

The above discussions illustrate exciting progress in pursuing the extremes of heat conduction materials. Below we offer some thoughts on future directions. With the maturity of first-principles based method, the high-throughput screening of materials with extreme thermal conductivities now become possible.[125] So far, however, the DFT and BTE based first-principles methods work well only for single crystals. Effects of defects, interfaces, and nanostructure distributions on heat conduction cannot be dealt with confidence, partly owing to the lack of knowledge in the details of such imperfections in practical materials. Machine learning of microscopic structures combined with predictive modeling of heat conduction may be a fruitful direction to pursue, especially for high-fidelity modeling of phonon transport at extreme conditions,[126] amorphous materials[127], as well as the structural design of maximized/minimized thermal resistance of superlattices[128] and even polymers.[129] For fast screening of materials, convenient and high-throughput thermal measurement tools are necessary.[130] While optical pump-probe methods have been successfully used to study nanoscale films and bulk materials, certain materials such as stretched polymer films pose challenges owing to their uneven sample surfaces and crystallites that strongly scatter the optical beam. Weak optical absorption in the visible spectrum for polymers and large band-gap materials poses another challenge, though this can be resolved by extending to ultraviolet and infrared spectra.

There is a growing interest to dynamically adjust thermal properties on-demand, much as one can control the flow of electrons in electronic circuits. Progress has been made, for example, using ion intercalation,[131] phase transition, or structural transformation such as polymer-hydration,[132] electric field-induced ferroelectric domain orientation[133], and light-induced phase change.[134] The maximum contrast achieved so far (~10±4) is still relatively small and typically on small pieces

of materials.[135] For practical applications such as for building envelopes and thermal energy storage, which most likely will call for thermal insulation in one case and heat conduction in another, larger contrasts (at least 10 on/off ratio) and low cost are needed.[136] Whereas switchable mechanical contacts can change the thermal resistance from one limited by interfacial resistance to that of vacuum gap with a contrast ratio of ~2000, [137] the process is slow and inconvenient due to the mechanical motion. A great challenge is to achieve a similar contrast in the thermal conductivity without macroscopic mechanical motions. One possible way is to explore thermal conductivity switch in phase change materials. For example, the on/off ratio close to 8 is found in phase change $Ge_2Sb_2Te_5$,[138] but cyclability remains challenging.

Besides room-temperature applications, many energy-related applications call for extreme thermal properties under extreme conditions. For example, thermal barrier coatings that can withstand over 1000 ℃ for gas turbines has been under active development for a long time, with yttria-stabilized zirconia representing the state-of-art material with thermal conductivity of ~2.5 W/m-K at 1000 ℃.[57] More recent activities in hypersonic vehicles and ultrahigh temperature energy storage systems call for thermal insulation materials that can endure high temperature and oxidative environment.[139] At these temperatures, radiation contributions to heat transfer in solids become significant. Simulating and reliably measuring their properties at extreme working conditions pose both theoretical and experimental challenges.

Finally, the thermal transport properties of materials are often only part of the important factors to consider in practical applications. Simultaneous optimization of multiple properties is often required for real applications. Thermal expansion coefficient, for example, is equally important when considering bonding different materials together. The thermoelectric figure of merit, which requires high electrical conductivity, large Seebeck coefficient, and low thermal conductivity is an excellent example of such simultaneous optimization. With the recent advancement in first-principles simulation methods, computing material properties considering the interactions between electrons, phonons, and photons become available. This will enable the simultaneous optimization of thermal, electrical, and optical properties for multifunctional materials, and further improvement of material performance for thermal energy conversion.

Box 1 | Phonon heat conduction in crystalline and disordered solids

For crystalline solids, Peierls showed that heat transport can be understood as the propagation of phonons and their scatterings among each other. The three phonon processes are the lowest order and usually the strongest scattering processes, and can be grouped into normal or Umklapp scattering that conserves or destroys the crystal momentum respectively, with the latter creating the intrinsic thermal resistance. By identifying the characteristic timescale (known as the relaxation time or lifetime) τ at which phonon scattering events occur, the thermal conductivity of a solid material can be generally written as an integration over the phonon spectrum:

$$k = \frac{1}{3}\int \hbar\omega N(\omega)\frac{\partial f}{\partial T} v^2(\omega)\tau(\omega)d\omega = \frac{1}{3}\int C(\omega)v^2(\omega)\tau(\omega)d\omega \quad (2)$$

where the integration $\int d\omega$ is integrating over the entire phonon spectrum and summing over all polarizations, v is the phonon group velocity and $C(\omega) = \hbar\omega N(\omega)\frac{\partial f}{\partial T}$ is the spectral volumetric specific heat, where f is the Bose-Einstein distribution and $N(\omega)$ is the density of states. The typical temperature dependence of thermal conductivity $k(T)$ of crystals is shown in Fig.B1a. In the high-temperature regime, the thermal conductivity decreases with absolute temperature approximately following T^{-n}, with n =1 expected due to intrinsic phonon-phonon scattering rates approximately proportional to T. At low temperatures also known as the Casimir regime, the scattering is limited by the sample size because phonon-phonon scatterings are much weaker, and $k{\sim}T^3$ is expected. Typical phonon scattering mechanisms including phonon scatterings by other phonons and defects are summarized in Fig. B1b.

Contrary to crystals, disordered solids lack the periodicity, rendering the PGM no longer applicable. For example, Fig. B1c showed drastically different $k(T)$ behavior of amorphous silicon compared with crystals. Thermal conductivity of amorphous materials increases quadratically with temperature, followed by a plateau and then a slow increase. Although the picture of tunneling across the double-well potential of a two-level system had been proposed to explain the low-temperature thermal conductivity,[140] the heat conduction mechanisms in amorphous materials have not settled. Allen and Feldman provided a quantitative theory for harmonic disordered solids based on the quantum picture of degenerate mode transitions. Allen-Feldman theory showed that atomic vibrations in disordered materials can be categorized into three types: "propagons" that are phonon-like propagating waves, "diffusons" that can be regarded as random walkers, and "locons" that are spatially localized, as shown in Fig.B1d.[141] Thermal conductivity of these three types of vibrational modes are written as a spectral integral as well:

$$k = \int C(\omega)D(\omega)d\omega \quad (3)$$

where $D(\omega)$ is the spectral diffusivity at frequency ω.[3] For propagons, $D(\omega) = v^2(\omega)\tau(\omega)/3$, similar to the PGM, while locons have zero mode diffusivity $D = 0$ (when ignoring anharmonic interactions), as shown Fig.B1d. Allen-Feldman theory provided a unified picture for explaining the temperature-dependent thermal conductivity below and above the plateau, due to transition from propagon-dominant to the diffuson-dominant regime (Fig. B1c).

In the view of Allen-Feldman theory, a material with low thermal conductivity should ideally support locons as the majority of vibrational modes with minimal interactions among them. Slack[32] and Cahill et al.[142] also proposed minimum thermal conductivity (k_{min}) theory of disordered solid based on based on PGM, assuming that the phonon mean free paths (MFP, $\Lambda = v\tau$) cannot be smaller than one or half of phonon wavelength, respectively. However, experiments in layered materials[29] and fullerene derivatives[121,143] have shown that thermal conductivities lower than k_{min} can be achieved. Phenomena such

as total internal reflection, phonon confinement[82] and phonon focusing effect due to anisotropy[144] can lead to thermal conductivity lower than k_{min}.

Figure B1. Thermal conductivity and energy carriers in crystalline and amorphous materials. a. Typical temperature-dependent thermal conductivity of semiconductor Si, showing different scattering mechanisms in different temperature ranges. Replotted based on ref. [145], copyright by American Physical Society 1964. C**b**. Schematic of phonon scattering mechanisms. **c**. Temperature-dependent thermal conductivity of amorphous silicon including the diffuson and propagon contributions[141], compared with measurements by Pompe[146] and Cahill[147,148] **d.** Schematic of locons, diffusons and propagons, and spectral mode diffusivity in a-Si.[141] Part d and e are replotted based on ref[141], copyright by Taylor and Francis Online, copyright by Taylor and Francis Online 1999.

Box 2 | Developments of first-principles phonon modeling

While specific heat $C(\omega)$ and group velocity $v(\omega)$ in the PGM of thermal conductivity can be computed from the phonon dispersion using harmonic lattice dynamics, the relaxation time $\tau(\omega)$ depends on anharmonic multi-phonon interactions. Klemens developed approximate expressions for $\tau(\omega)$ with coefficients determined by empirically fitting the experimental data, using simplified phonon dispersion relations such as the Debye model.[4] This widely used approach lacks predictive power. The situation started to change in the 1990s. The development of density functional perturbation theory (DFPT) enabled determining phonon dispersions $\omega(\boldsymbol{q}, s)$ once the elements and lattice structure are known.[150] The next component towards determining k is the anharmonic force constants, which are related to the phonon relaxation time $\tau(\omega)$ via Fermi's golden rule.[151] From 1995, calculations of anharmonic line-widths and frequency shifts of phonon dispersion were reported.[152] With these necessary components, Broido et al. reported the first fully *ab initio* calculations of intrinsic thermal conductivity of crystalline Si,[11] with excellent agreement with the experiment without adjustable parameters. Now first-principles phonon modeling is routinely used for thermal conductivity prediction.[153] Fig B2a summarizes the workflow of first-principles phonon calculations, by starting from DFT to obtain harmonic and anharmonic force constants, and then deriving harmonic and anharmonic phonon properties and finally thermal conductivity. Fig B2b shows the comparison of first-principles prediction and experimental values for several typical semiconductors.

The power of first-principles phonon modeling not only lies in its accuracy in predicting thermal conductivity, but also the detailed insights it provides on phonon interaction events. The accumulative thermal conductivity is usually used to resolve the MFPs of dominant heat-carrying phonons, which is defined as:[154,155]

$$k(\Lambda) = \frac{1}{3}\int C(\omega)v(\omega)\Lambda(\omega)\cdot\theta\big(\Lambda-\Lambda(\omega)\big)d\omega \qquad (4)$$

where $\theta\big(\Lambda-\Lambda(\omega)\big)$ is the Heaviside step function that excludes phonons with MFPs greater than Λ from integration. Fig B2c shows the accumulative thermal conductivity normalized by the bulk value k_{bulk} of a few semiconductors calculated from first-principles. Clearly, phonon MFP is intrinsically broadband in nature. For example, phonons with MFPs longer than 1 μm contribute to nearly half of thermal conductivity in Si at room temperature.[156] Such understanding lays the foundation of tailoring lattice thermal conductivity through manipulating phonon scattering strengths. In addition to thermal conductivity prediction, first-principles calculations have also been used to study the hydrodynamic transport regime,[157,158] when normal scattering is the dominant scattering process. For example, second sound above 100 K was predicted in graphite and confirmed by TTG experiment.[28]

First-principles phonon modeling remains an active topic in computational physics and heat transfer. In addition to perfect crystals, the phonon-alloy scattering effect on thermal conductivity has also been included using virtual crystal approximation and perturbation theory for mass-disorder scatterings.[65] Coupling BTE with other modeling tools such as atomistic Green's function[12] further enabled modeling and engineering phonon transport in nanostructured materials, such as "nanoparticles in alloys".[159] Recent developments of computing fourth-order anharmonic force constants provided insights contradicting to "textbook" beliefs that four-phonon scatterings are negligible.[36] Four-phonon scatterings can considerably limit the thermal conductivity in BAs and graphene.[36] Higher-order force constants could also be important in studying phonon dispersions and thermodynamic properties at high temperatures.[160] Finally, First-principles calculation has also been extended to study coupled multi-carrier transport such as electron-phonon interaction, providing important insights for energy and current transport in electronic, thermoelectric, and photovoltaic devices. Electron-phonon interaction and their coupled transport are studied by solving the coupled electron's and phonon's BTE using DFT derived scattering matrices. Recent studies found that electron-phonon coupling could significantly contribute to thermal resistances at high carrier concentrations.[161] Electron-phonon interaction might also affect thermoelectric properties, for example, the Seebeck coefficient could also be enhanced through the phonon-drag effect.[162]

Fig. B2. First-principles prediction of thermal conductivity and phonon properties. a. Workflow of first-principles phonon modeling. The potential energy is written as Taylor expansions of displacements (u_i^α) with respect the equilibrium potential U_0, with the second and third-order derivatives referred as harmonic force constants (FC2, $\phi_{ij}^{\alpha\beta}$), third-order force constants (FC3, $\chi_{ijk}^{\alpha\beta\gamma}$) and forth-order force constants(FC4, $\chi_{ijkl}^{\alpha\beta\gamma\delta}$). FC2 are used to perform lattice dynamics to derive phonon dispersions, group velocities $v(\omega)$, and specific heat $C(\omega)$. C3 and sometimes FC4 are used for computing relaxation time $\tau(\omega)$ based on Fermi's golden rule. **b**. Temperature-dependent thermal conductivity by first-principles predictions (lines) compared with experimental data. Modified based on ref.[163], Copyright by American Institute of Physics 2019. **c**. First-principles prediction of accumulative thermal conductivity as a function of phonon MFP. The data for half-Heusler compound ZrCoSb is taken from ref. [164], others are our first-principles modeling data.

Box 3 | Advances in thermal metrologies

Thermal conductivity is difficult to measure. Commercial equipment such as laser flash and hot plate methods are suitable for large samples. A range of experimental methods has been developed to characterize small bulk, film, and nanowire samples. The 3ω method (Fig B3a) uses a microfabricated metallic line as the heater with a sinusoidal heat input voltage at the frequency ω and detects the third harmonics in voltage at 3ω to determine its temperature rise. The 3ω method has the advantage of being insensitive to radiation heat loss at even 1000 K, [165], and is primarily used to determine the cross-plane thermal conductivity of thin films. The 3ω method can also measure the in-plane thermal conductivity through changing heater width or heating frequency.[166] Thermal conductivity measurements of nanowires and nanotubes often employ microfabricated suspended island structures as shown in Fig.B3b with heaters/temperature sensors fabricated on each island. [48] Such structures have high thermal resistance to the environment. When one island is heated up, heat flows along the nanowire/nanotube to the other island. By measuring the temperature rises on both islands, the thermal conductivity of the nanowire/nanotube can be determined. Fabricating these testing structures requires access to cleanrooms, and the placement of nanowire/nanotube across the suspended island imposes additional challenges.

In comparison, non-contact optical methods require minimal sample preparations. Among these methods, mostly used are pump-probe techniques such as time-domain[167] and frequency-domain thermoreflectance (TDTR and FDTR),[168] and transient thermal grating (TTG).[169] FDTR and TDTR are versatile characterization techniques capable of measuring multiple thermal properties including thermal conductivity, interface conductance, and specific heat.[170] TDTR and FDTR uses a pump laser to heat the sample coated with a transducer film, and a probe laser to detect the reflectance change caused by the transient heating of the pump laser (Fig B3c). As shown in Fig B3d and Fig B3e, the TDTR method is based on pulsed laser heating, and measure the reflectance change as a function of the delay time between the pump and the probe beams, while the FDTR method is usually based on modulated continuous wave laser heating and the reflectance signal is measured as a function of the heating frequency. These two methods require less sample preparations, involving only deposition of a metal thin film as the transducer. Recent developments showed that even transducer layer can be removed for opaque samples, which greatly increases sensitivity to the in-plane thermal transport.[171] TTG, on the other hand, uses two crossed pump-beam interfering with each other, creating a sinusoidal thermal grating on the sample (Fig B3f). The probe light will in turn be diffracted by the thermal grating. TTG is primarily sensitive to in-plane thermal conductivity, and does not require any transducer deposition. Furthermore, it was discovered when the heater size, e.g. laser beam diameter,[16] thermal penetration depth, [172] or grating spacing[173] are comparable to the phonon MFPs, the measured thermal conductivity is reduced even though there are no physical boundaries to scatter phonons. This phenomenon has been exploited to extract the accumulative thermal conductivity over the MFP spectrum, making it possible to spectrally probe non-diffusive phonon transport and validate first-principles simulations (Fig B3g). Recent advances in pump-probe techniques further allow spectrally resolving phonon transmission at interfaces, [174] and electron-phonon interaction,[175,176] which provided understanding of scattering and transport of energy-carriers on the spectral level.

Fig B3. Experimental techniques for characterizing thermal conductivity and phonon MFP. a. Schematic of 3ω method for thermal conductivity measurement of thin films. **b**. SEM of a microfabricated island platform for measuring the thermal conductivity of suspended 1D nanostructures. Reprinted from [48], copyright by American Physical Society 2001. **c-e.** Schematic of TDTR and FDTR measurements. **c**. Multilayered sample configuration and pump and probe lasers. **d**. Pump heating power of TDTR and FDTR. TDTR uses modulated pulsed laser while FDTR usually uses CW pulses. **e**. Schematic of TDTR and FDTR signals. TDTR measures the thermal phase lag as a function of the delay time of probe pulses, while FDTR measures the phase as a function of modulation frequency. **f**. Schematic of transient thermal grating

technique, reprinted from ref.[173], copyright by American Physical Society 2013. **g**. Experimentally reconstructed accumulative thermal conductivity (symbols)[177], compared with first-principles prediction (lines).

Acknowledgments: This review is built on the work of the community and many former students/post-docs and collaborators the senior author had worked with; and financial support from the Office of Naval Research under Multidisciplinary University Research Initiative grant N00014-16-1-2436 (for high thermal conductivity materials), and U.S. Department of Energy(DOE)–Basic Energy Sciences (Award No. DE-FG02-02ER45977 (polymers), MRSEC Program of the National Science Foundation under award number DMR-1419807 (oxides and thermal regulation), and NSF under award CBET 1851052 (thermal metrology).

Competing interests

The authors declare no competing interests.

References

1 Kittel, C. *Introduction to Solid State Physics 7th Ed*. (Wiley, 1996).

2 Peierls, R. Zur kinetischen Theorie der Wärmeleitung in Kristallen. *Ann. Phys. (Leipzig)* **395**, 1055-1101, (1929).

3 Allen, P. B. & Feldman, J. L. Thermal conductivity of disordered harmonic solids. *Phys. Rev. B* **48**, 12581-12588, (1993).

4 Klemens, P. G. The scattering of low-frequency lattice waves by static imperfections. *Proc. Phys. Soc., Section A* **68**, 1113, (1955).

5 Callaway, J. Model for Lattice Thermal Conductivity at Low Temperatures. *Phys. Rev.* **113**, 1046-1051, (1959).

6 Cahill, D. G. *et al.* Nanoscale thermal transport. *J. Appl. Phys.* **93**, 793, (2003).

7 Cahill, D. G. *et al.* Nanoscale thermal transport. II. 2003–2012. *Applied Physics Reviews* **1**, 011305, (2014).

8 Dresselhaus, M. S. *et al.* New Directions for Low-Dimensional Thermoelectric Materials. *Adv. Mater.* **19**, 1043-1053, (2007).

9 Volz, S. G. & Chen, G. Molecular-dynamics simulation of thermal conductivity of silicon crystals. *Phys. Rev. B* **61**, 2651, (2000).

10 McGaughey, A. J. H. & Larkin, J. M. Predicting Phonon Properties from Equilibrium Molecular Dynamics Simulations. *Annual Review of Heat Transfer* **17**, 49-87, (2014).

11 Broido, D. A., Malorny, M., Birner, G., Mingo, N. & Stewart, D. A. Intrinsic lattice thermal conductivity of semiconductors from first principles. *Appl. Phys. Lett.* **91**, 231922, (2007).

12 Zhang, W., Fisher, T. S. & Mingo, N. The Atomistic Green's Function Method: An Efficient Simulation Approach for Nanoscale Phonon Transport. *Numerical Heat Transfer, Part B: Fundamentals* **51**, 333-349, (2007).

13 Marcolongo, A., Umari, P. & Baroni, S. Microscopic theory and quantum simulation of atomic heat transport. *Nature Physics* **12**, 80-84, (2015).

14 Bartok, A. P., Payne, M. C., Kondor, R. & Csanyi, G. Gaussian approximation potentials: the accuracy of quantum mechanics, without the electrons. *Phys. Rev. Lett.* **104**, 136403, (2010).

15 Dai, J. & Tian, Z. Rigorous formalism of anharmonic atomistic Green's function for three-dimensional interfaces. *Phys. Rev. B* **101**, 041301(R), (2020).

16 Minnich, A. J. *et al.* Thermal Conductivity Spectroscopy Technique to Measure Phonon Mean Free Paths. *Phys. Rev. Lett.* **107**, 095901, (2011).

17 Siemens, M. E. *et al.* Quasi-ballistic thermal transport from nanoscale interfaces observed using ultrafast coherent soft X-ray beams. *Nat Mater* **9**, 26-30, (2010).

18 Kang, J. S., Li, M., Wu, H., Nguyen, H. & Hu, Y. Experimental observation of high thermal conductivity in boron arsenide. *Science* **361**, 575-578, (2018).

19 Tian, F. *et al.* Unusual high thermal conductivity in boron arsenide bulk crystals. *Science* **361**, 582-585, (2018).

20 Li, S. *et al.* High thermal conductivity in cubic boron arsenide crystals. *Science* **361**, 579-581, (2018).

21 Seyf, H. R. *et al.* Rethinking phonons: The issue of disorder. *npj Computational Materials* **3**, 49, (2017).
22 Kim, W. *et al.* Thermal conductivity reduction and thermoelectric figure of merit increase by embedding nanoparticles in crystalline semiconductors. *Phys. Rev. Lett.* **96**, 045901, (2006).
23 Poudel, B. *et al.* High-thermoelectric performance of nanostructured bismuth antimony telluride bulk alloys. *Science* **320**, 634-638, (2008).
24 Luckyanova, M. N. *et al.* Coherent Phonon Heat Conduction in Superlattices. *Science* **338**, 936-939, (2012).
25 Ravichandran, J. *et al.* Crossover from incoherent to coherent phonon scattering in epitaxial oxide superlattices. *Nat Mater* **13**, 168-172, (2014).
26 Luckyanova, M. N. *et al.* Phonon localization in heat conduction. *Science Advances* **4**, eaat9460, (2018).
27 Fermi, E., Pasta, P., S, U. & Tsingou, M. *Studies of the nonlinear problems*. (United States: N. p., 1955).
28 Huberman, S. *et al.* Observation of second sound in graphite at temperatures above 100 K. *Science* **364**, 375-379, (2019).
29 Chiritescu, C. *et al.* Ultralow thermal conductivity in disordered, layered WSe2 Crystals. *Science* **315**, 351-353, (2007).
30 Vaziri, S. *et al.* Ultrahigh thermal isolation across heterogeneously layered two-dimensional materials. *Science Advances* **5**, eaax1325, (2019).
31 Srivastava, G. P., Singh, D. P. & Verma, G. S. Three-Phonon Scattering Strengths and Ziman Limit of Resistivity Due to Three-Phonon Scattering Processes in Ge. *Phys. Rev. B* **6**, 3053-3055, (1972).
32 Slack, G. A. Nonmetallic Crystals with High Thermal Conductivity. *J. Phys. Chem. Solids* **34**, 321-335, (1973).
33 Chen, K. *et al.* Ultrahigh thermal conductivity in isotope-enriched cubic boron nitride. *Science* **367**, 555-559, (2020).
34 Morelli, D. T. & Slack, G. A. in *High thermal conductivity materials, Chapter 2* 37-68 (2005).
35 Lindsay, L., Broido, D. A. & Reinecke, T. L. First-principles determination of ultrahigh thermal conductivity of boron arsenide: a competitor for diamond? *Phys. Rev. Lett.* **111**, 025901, (2013).
36 Feng, T., Lindsay, L. & Ruan, X. Four-phonon scattering significantly reduces intrinsic thermal conductivity of solids. *Phys. Rev. B* **96**, 161201(R), (2017).
37 Dames, C. Ultrahigh thermal conductivity confirmed in boron arsenide. *Science* **361**, 549-550, (2018).
38 Giri, A. & Hopkins, P. Achieving a better heat conductor. *Nat. Mater.* **19**, 481-490, (2020).
39 Kang, J. S., Wu, H. & Hu, Y. Thermal Properties and Phonon Spectral Characterization of Synthetic Boron Phosphide for High Thermal Conductivity Applications. *Nano Lett* **17**, 7507-7514, (2017).
40 Qian, X., Jiang, P. & Yang, R. Anisotropic thermal conductivity of 4H and 6H silicon carbide measured using time-domain thermoreflectance. *Materials Today Physics* **3**, 70-75, (2017).

41 Ravichandran, N. K. & Broido, D. Phonon-Phonon Interactions in Strongly Bonded Solids: Selection Rules and Higher-Order Processes. *Physical Review X* **10**, 021063, (2020).
42 Lv, B. *et al.* Experimental study of the proposed super-thermal-conductor: BAs. *Appl. Phys. Lett.* **106**, 074105, (2015).
43 Lindsay, L., Broido, D. A. & Reinecke, T. L. Phonon-isotope scattering and thermal conductivity in materials with a large isotope effect: A first-principles study. *Phys. Rev. B* **88**, 144306, (2013).
44 Zheng, Q. *et al.* Thermal conductivity of GaN, ^{71}GaN, and SiC from 150 K to 850 K. *Physical Review Materials* **3**, 014601, (2019).
45 Gu, X., Wei, Y., Yin, X., Li, B. & Yang, R. Colloquium: Phononic thermal properties of two-dimensional materials. *Rev. Mod. Phys.* **90**, 041002, (2018).
46 Lindsay, L., Broido, D. A. & Mingo, N. Lattice thermal conductivity of single-walled carbon nanotubes: Beyond the relaxation time approximation and phonon-phonon scattering selection rules. *Phys. Rev. B* **80**, 125407, (2009).
47 Lindsay, L., Broido, D. A. & Mingo, N. Flexural phonons and thermal transport in graphene. *Phys. Rev. B* **82**, 115427, (2010).
48 Kim, P., Shi, L., Majumdar, A. & McEuen, P. L. Thermal transport measurements of individual multiwalled nanotubes. *Phys. Rev. Lett.* **87**, 215502, (2001).
49 Maruyama, S. A molecular dynamics simulation of heat conduction in finite length SWNTs. *Physica B: Condensed Matter* **323**, 193-195, (2002).
50 Balandin, A. A. *et al.* Superior thermal conductivity of single-layer graphene. *Nano Lett.* **8**, 902-907, (2008).
51 Schmidt, A. J., Chen, X. & Chen, G. Pulse accumulation, radial heat conduction, and anisotropic thermal conductivity in pump-probe transient thermoreflectance. *Rev. Sci. Instrum.* **79**, 114902, (2008).
52 Mingo, N. & Broido, D. A. Length dependence of carbon nanotube thermal conductivity and the "problem of long wavelengths". *Nano Lett.* **5**, 1221-1225, (2005).
53 Lepri, S. Thermal conduction in classical low-dimensional lattices. *Physics Reports* **377**, 1-80, (2003).
54 Chang, C. W., Okawa, D., Garcia, H., Majumdar, A. & Zettl, A. Breakdown of Fourier's law in nanotube thermal conductors. *Phys. Rev. Lett.* **101**, 075903, (2008).
55 Xu, X. *et al.* Length-dependent thermal conductivity in suspended single-layer graphene. *Nature communications* **5**, 3689, (2014).
56 Takabatake, T., Suekuni, K., Nakayama, T. & Kaneshita, E. Phonon-glass electron-crystal thermoelectric clathrates: Experiments and theory. *Rev. Mod. Phys.* **86**, 669-716, (2014).
57 Clarke, D. R. & Phillpot, S. R. Thermal barrier coating materials. *Mater. Today* **8**, 22-29, (2005).
58 Weathers, A. *et al.* Glass-like thermal conductivity in nanostructures of a complex anisotropic crystal. *Phys. Rev. B* **96**, 214202, (2017).
59 Lee, S. *et al.* Resonant bonding leads to low lattice thermal conductivity. *Nature communications* **5**, 3525, (2014).
60 Delaire, O. *et al.* Giant anharmonic phonon scattering in PbTe. *Nat Mater* **10**, 614-619, (2011).

61 Christensen, M. *et al.* Avoided crossing of rattler modes in thermoelectric materials. *Nat Mater* **7**, 811-815, (2008).

62 Sales, B. C., Mandrus, D. & Williams, R. K. Filled Skutterudite Antimonides: A New Class of Thermoelectric Materials. *Science* **272**, 1325-1328, (1996).

63 Mukhopadhyay, S. *et al.* Two-Channel model for ultralow thermal conductivity of crystalline Tl_3VSe_4. *Science* **360**, 1445-1458, (2018).

64 Hoogeboom-Pot, K. M. *et al.* A new regime of nanoscale thermal transport: Collective diffusion increases dissipation efficiency. *Proc Natl Acad Sci U S A* **112**, 4846-4851, (2015).

65 Tian, Z. *et al.* Phonon conduction in PbSe, PbTe, and $PbTe_{1-x}Se_x$ from first-principles calculations. *Phys. Rev. B* **85**, 184303, (2012).

66 Li, C. W. *et al.* Orbitally driven giant phonon anharmonicity in SnSe. *Nature Physics* **11**, 1063-1069, (2015).

67 Ma, H. *et al.* Supercompliant and Soft $(CH_3NH_3)_3Bi_2I_9$ Crystal with Ultralow Thermal Conductivity. *Phys. Rev. Lett.* **123**, 155901, (2019).

68 Qian, X., Gu, X. & Yang, R. Lattice thermal conductivity of organic-inorganic hybrid perovskite $CH_3NH_3PbI_3$. *Appl. Phys. Lett.* **108**, 063902, (2016).

69 Pisoni, A. *et al.* Ultra-Low Thermal Conductivity in Organic–Inorganic Hybrid Perovskite CH3NH3PbI3. *J. Phys. Chem. Lett.* **5**, 2488-2492, (2014).

70 Zhu, T. & Ertekin, E. Mixed phononic and non-phononic transport in hybrid lead halide perovskites: glass-crystal duality, dynamical disorder, and anharmonicity. *Energy & Environmental Science* **12**, 216-229, (2019).

71 Ioffe, A. F. Semiconductor thermoelements and thermoelectric cooling. *PhT* **12**, 42, (1959).

72 Tamura, S. Isotope scattering of dispersive phonons in Ge. *Phys. Rev. B* **27**, 858-866, (1983).

73 Garg, J., Bonini, N., Kozinsky, B. & Marzari, N. Role of disorder and anharmonicity in the thermal conductivity of silicon-germanium alloys: a first-principles study. *Phys. Rev. Lett.* **106**, 045901, (2011).

74 Murakami, T., Shiga, T., Hori, T., Esfarjani, K. & Shiomi, J. Importance of local force fields on lattice thermal conductivity reduction in PbTe1–xSexalloys. *EPL (Europhysics Letters)* **102**, 46002, (2013).

75 Arrigoni, M., Carrete, J., Mingo, N. & Madsen, G. K. H. First-principles quantitative prediction of the lattice thermal conductivity in random semiconductor alloys: The role of force-constant disorder. *Phys. Rev. B* **98**, 115205, (2018).

76 Simoncelli, M., Marzari, N. & Mauri, F. Unified theory of thermal transport in crystals and glasses. *Nature Physics* **15**, 809-813, (2019).

77 Isaeva, L., Barbalinardo, G., Donadio, D. & Baroni, S. Modeling heat transport in crystals and glasses from a unified lattice-dynamical approach. *Nature communications* **10**, 3853, (2019).

78 Yang, R. & Chen, G. Thermal conductivity modeling of periodic two-dimensional nanocomposites. *Phys. Rev. B* **69**, 195316, (2004).

79 Casimir, H. B. G. Note on the conduction of heat in crystals. *Physica* **5**, 495-500, (1938).

80 Chen, G. Thermal conductivity and ballistic-phonon transport in the cross-plane direction of superlattices. *Phys. Rev. B* **57**, 14958, (1998).

81 Majumdar, A. Microscale Heat Conduction in Dielectric Thin Films. *J. Heat Transfer* **115**, 7-16, (1993).
82 Chen, G. Phonon Transport in Low Dimensional Structures. *Semiconductors and Semimetals, Chapter 5* **71**, 203, (2001).
83 Maire, J. *et al.* Heat conduction tuning by wave nature of phonons. *Science Advances* **3**, e1700027, (2017).
84 Venkatasubramanian, R. Lattice thermal conductivity reduction and phonon localizationlike behavior in superlattice structures. *Phys. Rev. B* **61**, 3091, (2000).
85 Chen, G. Phonon Wave Heat Conduction in Thin Films and Superlattices. *J. Heat Transfer* **121**, 945-953, (1999).
86 Yang, B. & Chen, G. Partially coherent phonon heat conduction in superlattices. *Phys. Rev. B* **67**, 195311, (2003).
87 Cuffe, J. *et al.* Reconstructing phonon mean-free-path contributions to thermal conductivity using nanoscale membranes. *Phys. Rev. B* **91**, 245423, (2015).
88 Liu, W. & Asheghi, M. Thermal Conductivity Measurements of Ultra-Thin Single Crystal Silicon Layers. *J. Heat Transfer* **128**, 75-83, (2006).
89 Asheghi, M., Leung, Y. K., Wong, S. S. & Goodson, K. E. Phonon-boundary scattering in thin silicon layers. *Appl. Phys. Lett.* **71**, 1798-1800, (1997).
90 Goodson, K. E. & Ju, Y. S. Heat conduction in novel electronic films. *Annu. Rev. Mater. Sci.* **29**, 261-293, (1999).
91 Li, D. *et al.* Thermal conductivity of individual silicon nanowires. *Appl. Phys. Lett.* **83**, 2934-2936, (2003).
92 Dames, C. & Chen, G. Theoretical phonon thermal conductivity of Si/Ge superlattice nanowires. *J. Appl. Phys.* **95**, 682-693, (2004).
93 Sperling, L. H. *Introduction to physical polymer science*. (John Wiley & Sons, 2005).
94 Henry, A. & Chen, G. High thermal conductivity of single polyethylene chains using molecular dynamics simulations. *Phys. Rev. Lett.* **101**, 235502, (2008).
95 Shulumba, N., Hellman, O. & Minnich, A. J. Lattice Thermal Conductivity of Polyethylene Molecular Crystals from First-Principles Including Nuclear Quantum Effects. *Phys. Rev. Lett.* **119**, 185901, (2017).
96 Shen, S., Henry, A., Tong, J., Zheng, R. & Chen, G. Polyethylene nanofibres with very high thermal conductivities. *Nature nanotechnology* **5**, 251-255, (2010).
97 Xu, Y. *et al.* Nanostructured polymer films with metal-like thermal conductivity. *Nature communications* **10**, 1771, (2019).
98 Choy, C. L., Wong, Y. W., Yang, G. W. & Kanamoto, T. Elastic modulus and thermal conductivity of ultradrawn polyethylene. *J. Polym. Sci., Part B: Polym. Phys.* **37**, 3359-3367, (1999).
99 Piraux, L., Kinany-Alaoui, M., Issi, J. P., Begin, D. & Billaud, D. Thermal conductivity of an oriented polyacetylene film. *Solid State Commun.* **79**, 427-429, (1989).
100 Shanker, A. *et al.* High thermal conductivity in electrostatically engineered amorphous polymers. *Science Advances* **3**, e1700342, (2017).
101 Xie, X. *et al.* High and low thermal conductivity of amorphous macromolecules. *Phys. Rev. B* **95**, 035406, (2017).

102 Miyazaki, Y., Nishiyama, T., Takahashi, H., Ktagiri, J.-i. & Takezawa, Y. in *2009 IEEE Conference on Electrical Insulation and Dielectric Phenoena, Virginia Beach, VA* 638-641 (2009).

103 Xu, Y. *et al.* Molecular Engineered Conjugated Polymer with High Thermal Conductivity. *Science Advances* **4**, eaar3031, (2018).

104 Liu, J. & Yang, R. Length-dependent thermal conductivity of single extended polymer chains. *Phys. Rev. B* **86**, 104307, (2012).

105 Zhang, T. & Luo, T. Morphology-influenced thermal conductivity of polyethylene single chains and crystalline fibers. *J. Appl. Phys.* **112**, 094304, (2012).

106 Zhang, T., Wu, X. & Luo, T. Polymer Nanofibers with Outstanding Thermal Conductivity and Thermal Stability: Fundamental Linkage between Molecular Characteristics and Macroscopic Thermal Properties. *J. Phys. Chem. C* **118**, 21148-21159, (2014).

107 Wang, X., Kaviany, M. & Huang, B. Phonon coupling and transport in individual polyethylene chains: a comparison study with the bulk crystal. *Nanoscale* **9**, 18022-18031, (2017).

108 Wang, X., Ho, V., Segalman, R. A. & Cahill, D. G. Thermal Conductivity of High-Modulus Polymer Fibers. *Macromolecules* **46**, 4937-4943, (2013).

109 Shrestha, R. *et al.* Crystalline polymer nanofibers with ultra-high strength and thermal conductivity. *Nature communications* **9**, 1664, (2018).

110 Singh, V. *et al.* High thermal conductivity of chain-oriented amorphous polythiophene. *Nature nanotechnology* **9**, 384-390, (2014).

111 Ronca, S., Igarashi, T., Forte, G. & Rastogi, S. Metallic-like thermal conductivity in a lightweight insulator: Solid-state processed Ultra High Molecular Weight Polyethylene tapes and films. *Polymer* **123**, 203-210, (2017).

112 Zhu, B. *et al.* Novel Polyethylene Fibers of Very High Thermal Conductivity Enabled by Amorphous Restructuring. *ACS Omega* **2**, 3931-3944, (2017).

113 Smith, M. K., Singh, V., Kalaitzidou, K. & Cola, B. A. Poly(3-hexylthiophene) Nanotube Array Surfaces with Tunable Wetting and Contact Thermal Energy Transport. *ACS Nano* **9**, 1080-1088, (2015).

114 Lu, C. *et al.* Thermal conductivity of electrospinning chain-aligned polyethylene oxide (PEO). *Polymer* **115**, 52-59, (2017).

115 Kurabayashi, K., Asheghi, M. & Goodson, K. E. Measurement of the thermal conductivity anisotropy in polyimide films. *Journal of Microelectromechanical Systems* **8**, 180-191, (1999).

116 Wei, X., Zhang, T. & Luo, T. Chain conformation-dependent thermal conductivity of amorphous polymer blends: the impact of inter- and intra-chain interactions. *Phys. Chem. Chem. Phys.* **18**, 32146-32154, (2016).

117 Kim, G. H. *et al.* High thermal conductivity in amorphous polymer blends by engineered interchain interactions. *Nat Mater* **14**, 295-300, (2015).

118 Cui, L. *et al.* Thermal conductance of single-molecule junctions. *Nature* **572**, 628-633, (2019).

119 Wang, Z. *et al.* Ultrafast Flash Thermal Conductance of Molecular Chains. *Science* **317**, 787-790, (2007).

120 Russ, B., Glaudell, A., Urban, J. J., Chabinyc, M. L. & Segalman, R. A. Organic thermoelectric materials for energy harvesting and temperature control. *Nature Reviews Materials* **1**, (2016).
121 Duda, J. C., Hopkins, P. E., Shen, Y. & Gupta, M. C. Exceptionally low thermal conductivities of films of the fullerene derivative PCBM. *Phys. Rev. Lett.* **110**, 015902, (2013).
122 Liu, J. *et al.* Ultralow thermal conductivity of atomic/molecular layer-deposited hybrid organic-inorganic zincone thin films. *Nano Lett.* **13**, 5594-5599, (2013).
123 Ong, W.-L. & Malen, J. A. Thermal Transport in Nanostructured Organic-Inorganic Hybrid Materials. *Annual Review of Heat Transfer* **19**, 67-126, (2016).
124 Yang, J. *et al.* Solution-Processable Superatomic Thin-Films. *J. Am. Chem. Soc.* **141**, 10967-10971, (2019).
125 van Roekeghem, A., Carrete, J., Oses, C., Curtarolo, S. & Mingo, N. High-Throughput Computation of Thermal Conductivity of High-Temperature Solid Phases: The Case of Oxide and Fluoride Perovskites. *Physical Review X* **6**, 041061, (2016).
126 Li, R., Lee, E. & Luo, T. A Unified Deep Neural Network Potential Capable of Predicting Thermal Conductivity of Silicon in Different Phases. *Materials Today Physics* **12**, 100181, (2019).
127 Qian, X., Peng, S., Li, X., Wei, Y. & Yang, R. Thermal conductivity modeling using machine learning potentials: application to crystalline and amorphous silicon. *Materials Today Physics* **10**, 100140, (2019).
128 Ju, S. *et al.* Designing Nanostructures for Phonon Transport via Bayesian Optimization. *Physical Review X* **7**, 021024, (2017).
129 Wu, S. *et al.* Machine-learning-assisted discovery of polymers with high thermal conductivity using a molecular design algorithm. *npj Computational Materials* **5**, 66, (2019).
130 Carrete, J., Li, W., Mingo, N., Wang, S. & Curtarolo, S. Finding Unprecedentedly Low-Thermal-Conductivity Half-Heusler Semiconductors via High-Throughput Materials Modeling. *Physical Review X* **4**, 011019, (2014).
131 Cho, J. *et al.* Electrochemically tunable thermal conductivity of lithium cobalt oxide. *Nature communications* **5**, 4035, (2014).
132 Tomko, J. A. *et al.* Tunable thermal transport and reversible thermal conductivity switching in topologically networked bio-inspired materials. *Nature nanotechnology* **13**, 959-964, (2018).
133 Ihlefeld, J. F. *et al.* Room-temperature voltage tunable phonon thermal conductivity via reconfigurable interfaces in ferroelectric thin films. *Nano Lett.* **15**, 1791-1795, (2015).
134 Shin, J. *et al.* Light-triggered thermal conductivity switching in azobenzene polymers. *Proc Natl Acad Sci U S A* **116**, 5973-5978, (2019).
135 Lu, Q. *et al.* Bi-directional tuning of thermal transport in SrCoOx with electrochemically induced phase transitions. *Nat Mater* **19**, 655-662, (2020).
136 Menyhart, K. & Krarti, M. Potential energy savings from deployment of Dynamic Insulation Materials for US residential buildings. *Building and Environment* **114**, 203-218, (2017).

137 Hao, M., Li, J., Park, S., Moura, S. & Dames, C. Efficient thermal management of Li-ion batteries with a passive interfacial thermal regulator based on a shape memory alloy. *Nature Energy* **3**, 899-906, (2018).
138 Lyeo, H.-K. *et al.* Thermal conductivity of phase-change material Ge2Sb2Te5. *Appl. Phys. Lett.* **89**, 151904, (2006).
139 Caccia, M. *et al.* Ceramic-metal composites for heat exchangers in concentrated solar power plants. *Nature* **562**, 406-409, (2018).
140 Anderson, P. w., Halperin, B. I. & Varma, c. M. Anomalous low-temperature thermal properties of glasses and spin glasses. *Philos. Mag.* **25**, 1-9, (1972).
141 Allen, P. B., Feldman, J. L., Fabian, J. & Wooten, F. Diffusons, locons and propagons: Character of atomie yibrations in amorphous Si. *Philos. Mag. B* **79**, 1715-1731, (1999).
142 Cahill, D., Watson, S. & Pohl, R. Lower limit to the thermal conductivity of disordered crystals. *Phys. Rev. B* **46**, 6131-6140, (1992).
143 Wang, X., Liman, C. D., Treat, N. D., Chabinyc, M. L. & Cahill, D. G. Ultralow thermal conductivity of fullerene derivatives. *Phys. Rev. B* **88**, 075310, (2013).
144 Chen, Z. & Dames, C. An anisotropic model for the minimum thermal conductivity. *Appl. Phys. Lett.* **107**, 193104, (2015).
145 Glassbrenner, C. J. & Slack, G. A. Thermal Conductivity of Silicon and Germanium from 3°K to the Melting Point. *Phys. Rev.* **134**, A1058-A1069, (1964).
146 Pompe, G. & Hegenbarth, E. Thermal conductivity of amorphous Si at low temperatures. *Physica Status Solidi B* **47**, 103-108, (1988).
147 Cahill, D. G., Fischer, H. E., Klitsner, T., Swartz, E. T. & Pohl, R. O. Thermal conductivity of thin films: Measurements and understanding. *Journal of Vacuum Science & Technology A: Vacuum, Surfaces, and Films* **7**, 1259-1266, (1989).
148 Cahill, D. G., Katiyar, M. & Abelson, J. R. Thermal conductivity of a-Si:H thin films. *Phys Rev B Condens Matter* **50**, 6077-6081, (1994).
149 Seyf, H. R. & Henry, A. A method for distinguishing between propagons, diffusions, and locons. *J. Appl. Phys.* **120**, 025101, (2016).
150 Giannozzi, P., de Gironcoli, S., Pavone, P. & Baroni, S. Ab initio calculation of phonon dispersions in semiconductors. *Phys Rev B Condens Matter* **43**, 7231-7242, (1991).
151 Ziman, J. M. *Electrons and Phonons: The Theory of Transport Phenomena in Solids*. (Oxford University Press, 2001).
152 Debernardi, A., Baroni, S. & Molinari, E. Anharmonic Phonon Lifetimes in Semiconductors from Density-Functional Perturbation Theory. *Phys. Rev. Lett.* **75**, 1819-1822, (1995).
153 Li, W., Carrete, J., A. Katcho, N. & Mingo, N. ShengBTE: A solver of the Boltzmann transport equation for phonons. *Comput. Phys. Commun.* **185**, 1747-1758, (2014).
154 Yang, F. & Dames, C. Mean free path spectra as a tool to understand thermal conductivity in bulk and nanostructures. *Phys. Rev. B* **87**, 035437, (2013).
155 Dames, C. & Chen, G. in *Thermoelectrics Handbook: Macro to Nano, Chapter 42* (ed D. M. Rowe) (Taylor & Francis Group, 2006).
156 Esfarjani, K., Chen, G. & Stokes, H. T. Heat transport in silicon from first-principles calculations. *Phys. Rev. B* **84**, 085204, (2011).
157 Lee, S., Broido, D., Esfarjani, K. & Chen, G. Hydrodynamic phonon transport in suspended graphene. *Nature communications* **6**, 6290, (2015).

158 Cepellotti, A. *et al.* Phonon hydrodynamics in two-dimensional materials. *Nature communications* **6**, 6400, (2015).
159 Mingo, N., Hauser, D., Kobayashi, N. P., Plissonier, M. & Shakouri, A. "Nanoparticle-in-Alloy" Approach to Efficient Thermoelectrics: Silicides in SiGe. *Nano Lett.* **9**, 711-715, (2009).
160 Tadano, T. & Tsuneyuki, S. Self-consistent phonon calculations of lattice dynamical properties in cubicSrTiO3with first-principles anharmonic force constants. *Phys. Rev. B* **92**, 054301, (2015).
161 Liao, B. *et al.* Significant reduction of lattice thermal conductivity by the electron-phonon interaction in silicon with high carrier concentrations: a first-principles study. *Phys. Rev. Lett.* **114**, 115901, (2015).
162 Zhou, J. *et al.* Ab initio optimization of phonon drag effect for lower-temperature thermoelectric energy conversion. *Proc Natl Acad Sci U S A* **112**, 14777-14782, (2015).
163 McGaughey, A. J. H., Jain, A. & Kim, H.-Y. Phonon properties and thermal conductivity from first principles, lattice dynamics, and the Boltzmann transport equation. *J. Appl. Phys.* **125**, 011101, (2019).
164 Shiomi, J., Esfarjani, K. & Chen, G. Thermal conductivity of half-Heusler compounds from first-principles calculations. *Phys. Rev. B* **84**, 104302, (2011).
165 Cahill, D. G. & Pohl, R. O. Thermal conductivity of amorphous solids above the plateau. *Phys. Rev. B* **35**, 4067-4073, (1987).
166 Dames, C. Measuring the thermal conductivity of thin films: 3 omega and related electrothermal methods. *Annual Review of Heat Transfer* **16**, 7-49, (2013).
167 Cahill, D. G. Analysis of heat flow in layered structures for time-domain thermoreflectance. *Rev. Sci. Instrum.* **75**, 5119-5122, (2004).
168 Schmidt, A. J., Cheaito, R. & Chiesa, M. A frequency-domain thermoreflectance method for the characterization of thermal properties. *Rev. Sci. Instrum.* **80**, 094901, (2009).
169 Maznev, A. A., Johnson, J. A. & Nelson, K. A. Onset of nondiffusive phonon transport in transient thermal grating decay. *Phys. Rev. B* **84**, 195206, (2011).
170 Jiang, P., Qian, X. & Yang, R. Tutorial: Time-domain thermoreflectance (TDTR) for thermal property characterization of bulk and thin film materials. *J. Appl. Phys.* **124**, 161103, (2018).
171 Qian, X., Ding, Z., Shin, J., Schmidt, A. J. & Chen, G. Accurate measurement of in-plane thermal conductivity of layered materials without metal film transducer using frequency domain thermoreflectance. *Rev. Sci. Instrum.* **91**, 064903, (2020).
172 Koh, Y. K. & Cahill, D. G. Frequency dependence of the thermal conductivity of semiconductor alloys. *Phys. Rev. B* **76**, 075207, (2007).
173 Johnson, J. A. *et al.* Direct measurement of room-temperature nondiffusive thermal transport over micron distances in a silicon membrane. *Phys. Rev. Lett.* **110**, 025901, (2013).
174 Hua, C., Chen, X., Ravichandran, N. K. & Minnich, A. J. Experimental metrology to obtain thermal phonon transmission coefficients at solid interfaces. *Phys. Rev. B* **95**, 205423, (2017).

175 Liao, B., Maznev, A. A., Nelson, K. A. & Chen, G. Photo-excited charge carriers suppress sub-terahertz phonon mode in silicon at room temperature. *Nature communications* **7**, 13174, (2016).

176 Zhou, J. *et al.* Direct observation of large electron-phonon interaction effect on phonon heat transport. *Nature communications* **11**, 6040, (2020).

177 Hu, Y., Zeng, L., Minnich, A. J., Dresselhaus, M. S. & Chen, G. Spectral mapping of thermal conductivity through nanoscale ballistic transport. *Nature nanotechnology* **10**, 701-706, (2015).

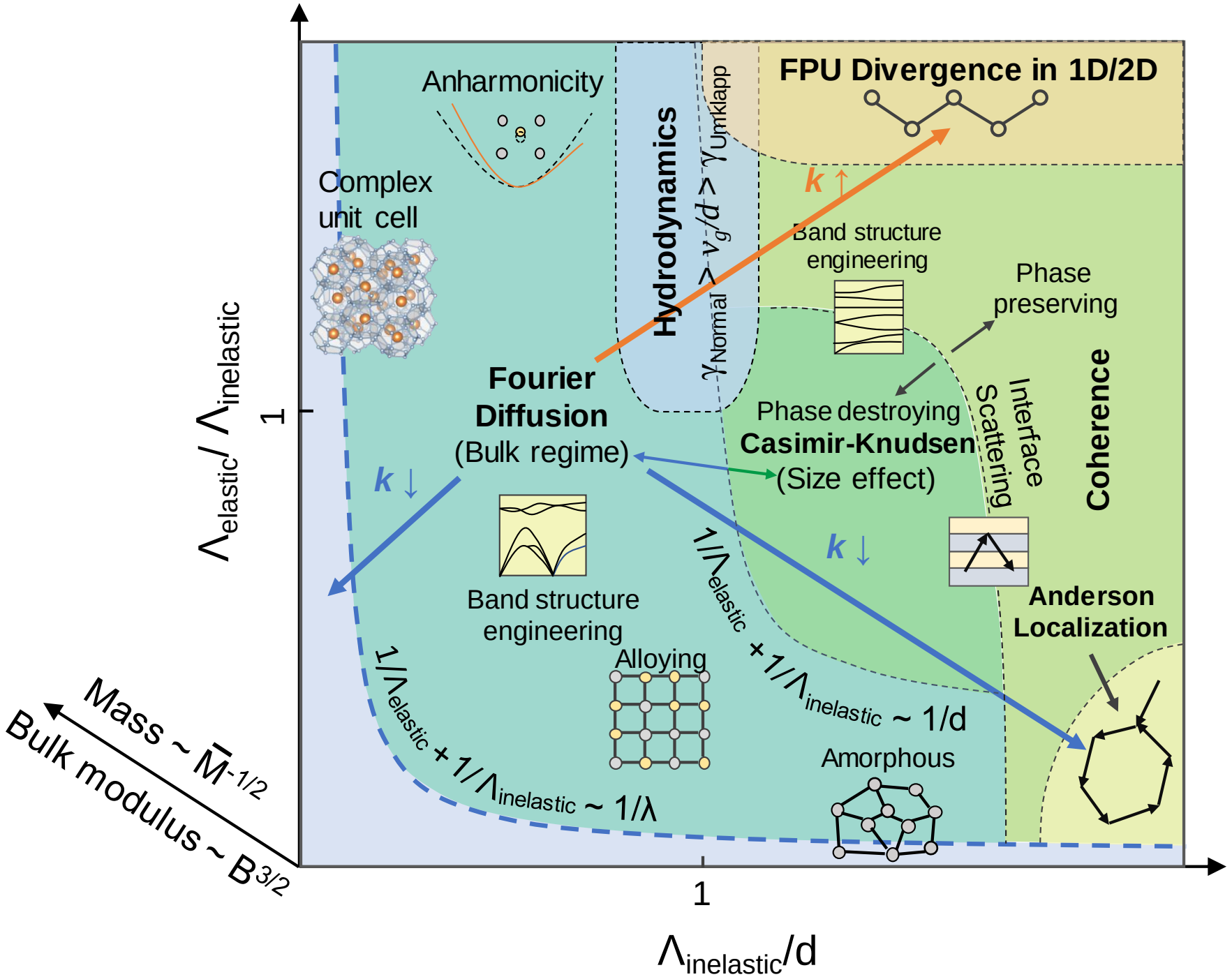
FPU Divergence in 1D/2D
Anharmonicity
Complex unit cell
Hydrodynamics
$\gamma_{Normal} > v_g/d > \gamma_{Umklapp}$
k ↑
Band structure engineering
Phase preserving
Fourier Diffusion
(Bulk regime)
Phase destroying
Casimir-Knudsen
(Size effect)
Interface Scattering
Coherence
k ↓
Band structure engineering
$1/\Lambda_{elastic} + 1/\Lambda_{inelastic} \sim 1/d$
k ↓
Anderson Localization
Alloying
$1/\Lambda_{elastic} + 1/\Lambda_{inelastic} \sim 1/\lambda$
Amorphous
$\Lambda_{elastic}/\Lambda_{inelastic}$
1
1
$\Lambda_{inelastic}/d$
Mass ~ $\bar{M}^{-1/2}$
Bulk modulus ~ $B^{3/2}$

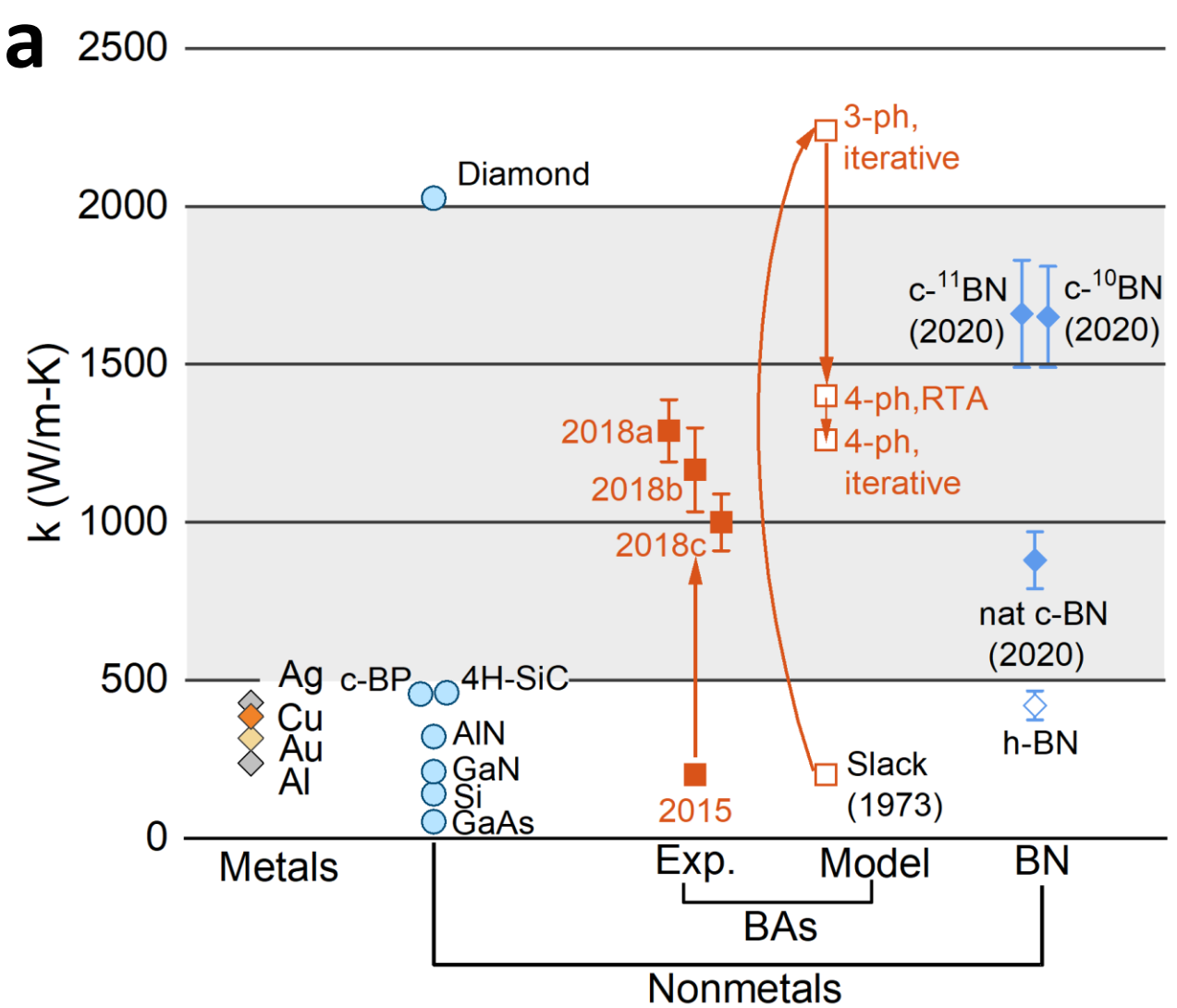
a
2500
2000
1500
1000
500
0
k (W/m-K)
Diamond
3-ph, iterative
c-11BN (2020)
c-10BN (2020)
2018a
2018b
2018c
4-ph,RTA
4-ph, iterative
nat c-BN (2020)
Ag
Cu
Au
Al
c-BP
4H-SiC
AlN
GaN
Si
GaAs
h-BN
2015
Slack (1973)
Metals
Exp.
Model
BN
BAs
Nonmetals

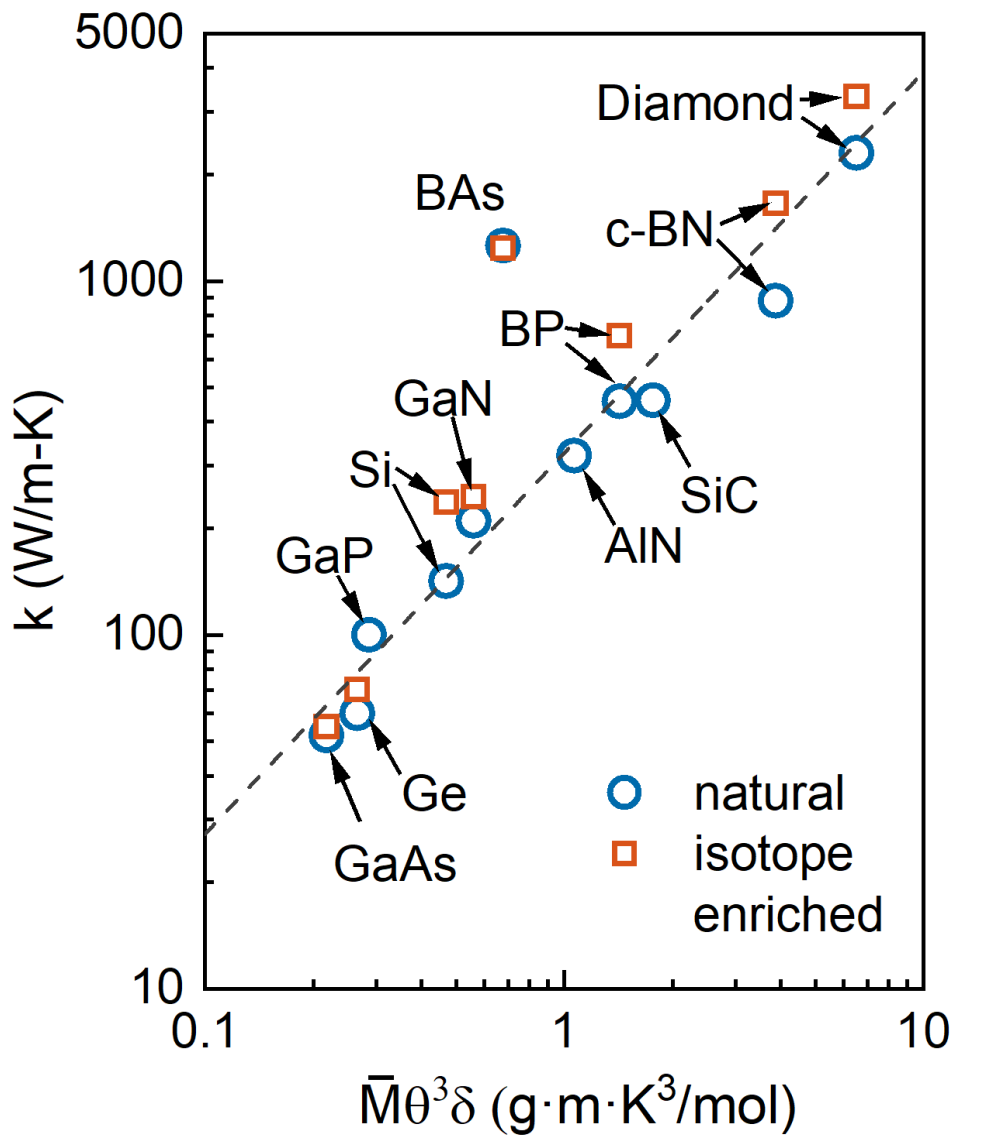
b
5000
1000
100
10
k (W/m-K)
Diamond
BAs
c-BN
BP
GaN
Si
SiC
AlN
GaP
Ge
GaAs
natural
isotope enriched
0.1
1
10
M̄θ³δ (g·m·K³/mol)

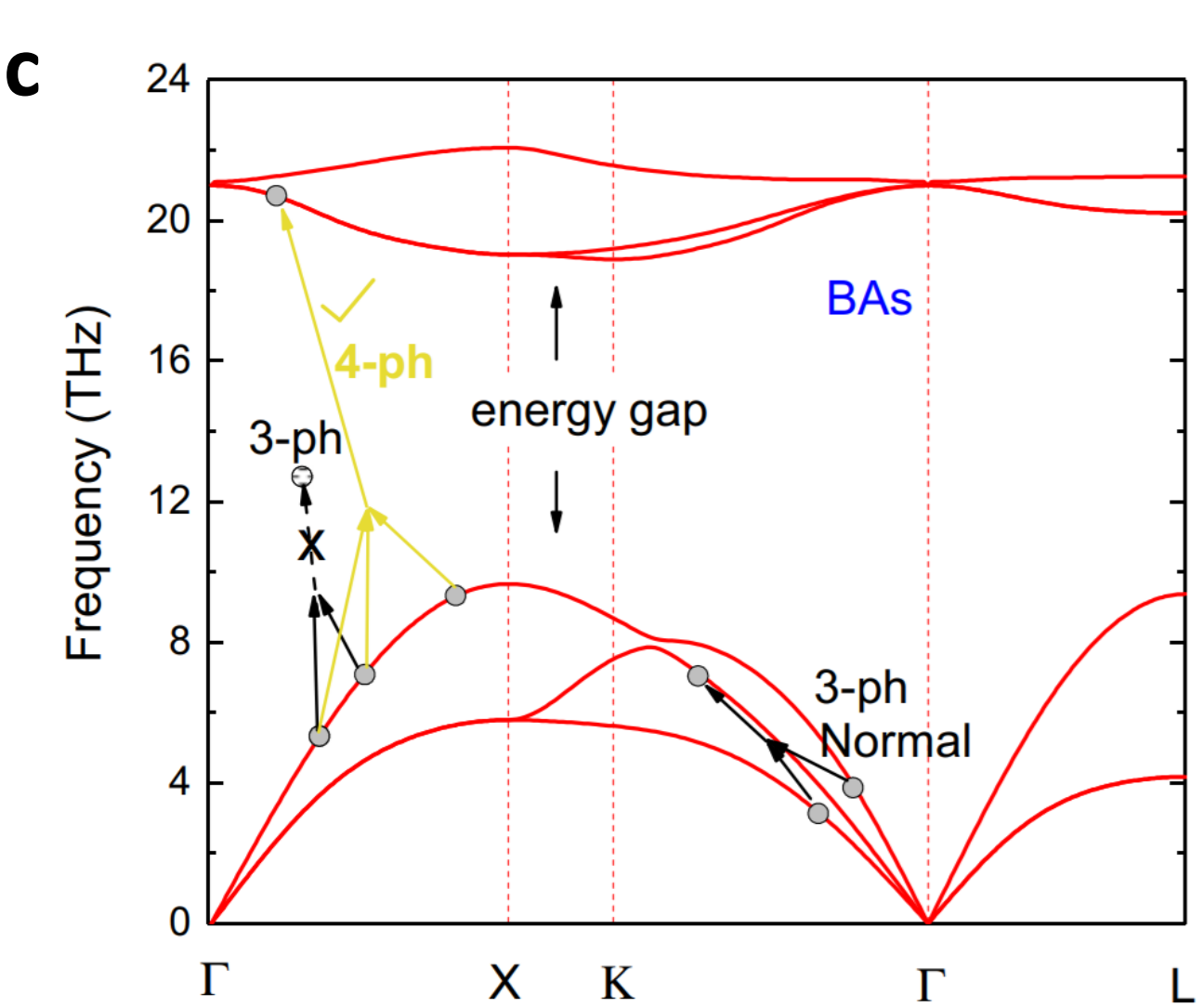
c
24
20
16
12
8
4
0
Frequency (THz)
BAs
4-ph
energy gap
3-ph
3-ph Normal
Γ
X
K
Γ
L

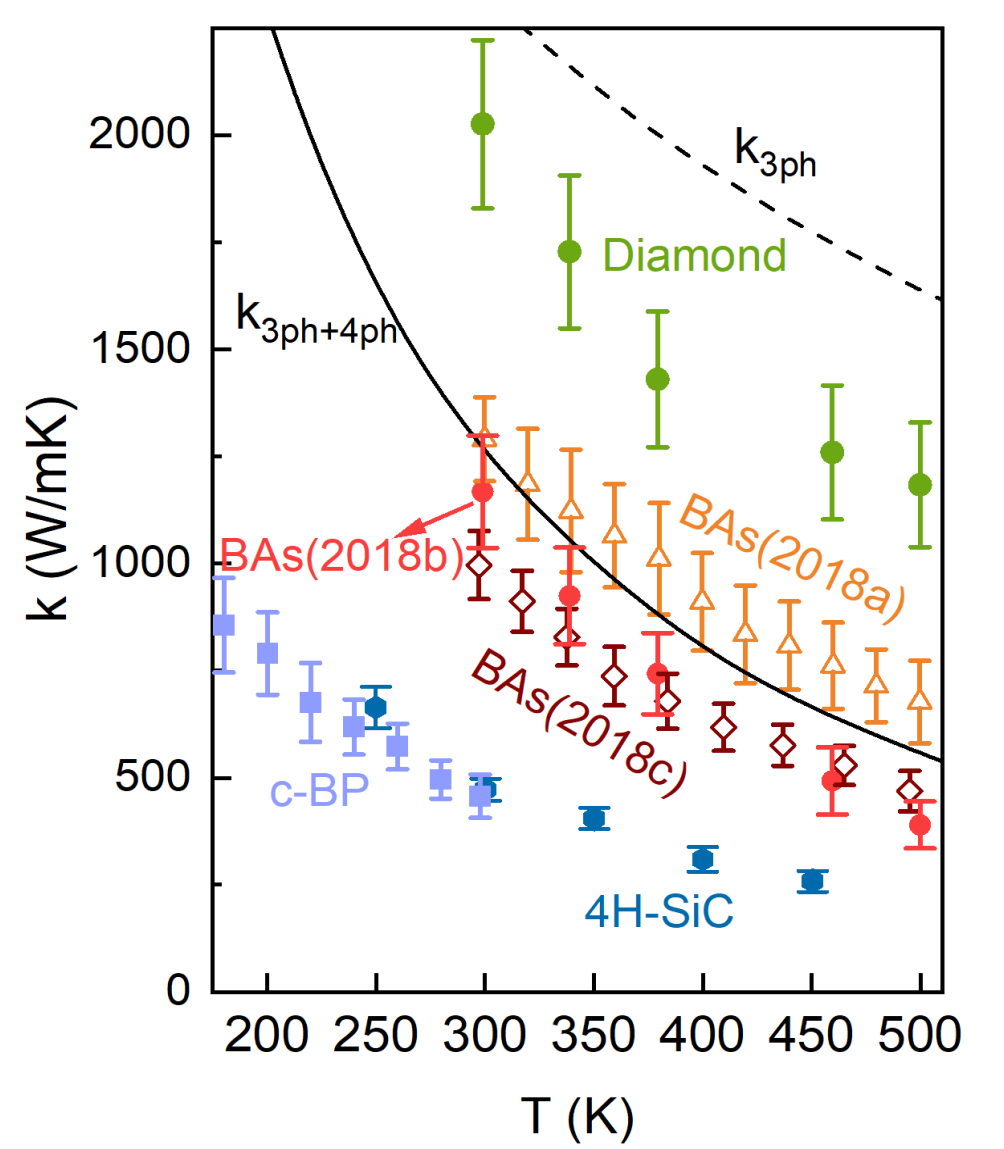
d
2000
1500
1000
500
0
k (W/mK)
k3ph
k3ph+4ph
Diamond
BAs(2018b)
BAs(2018a)
BAs(2018c)
c-BP
4H-SiC
200
250
300
350
400
450
500
T (K)

a. Materials design for intrinsically low-k

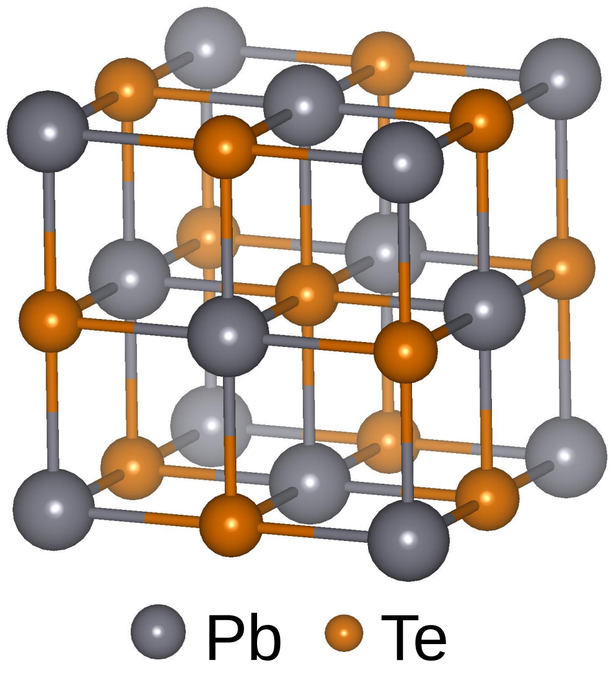

Heavy elements

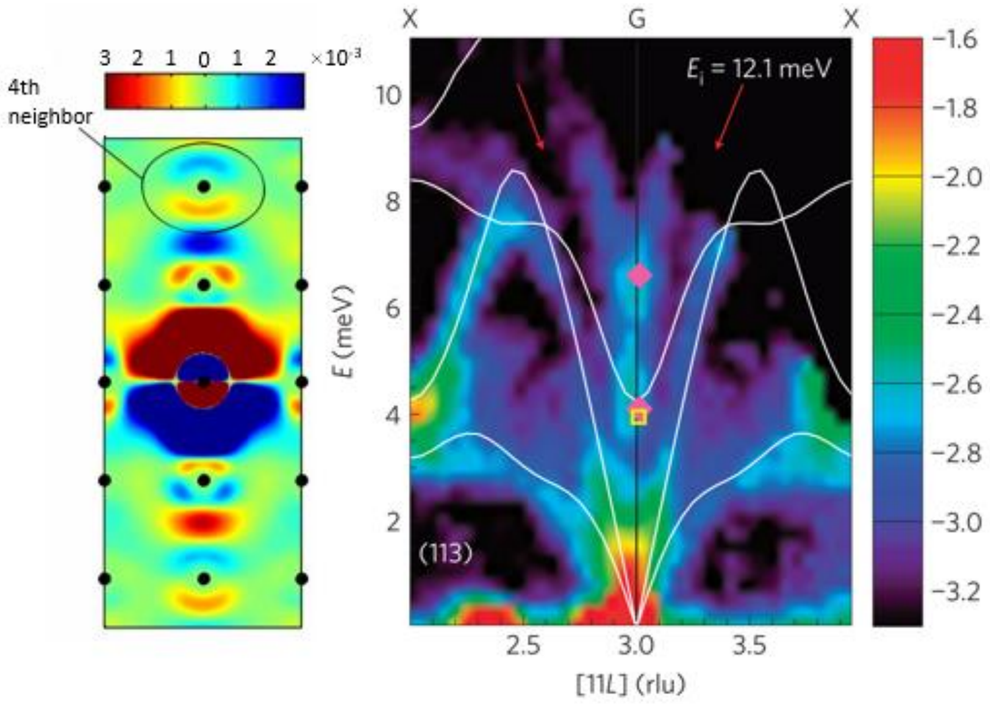

Strong anharmonicity

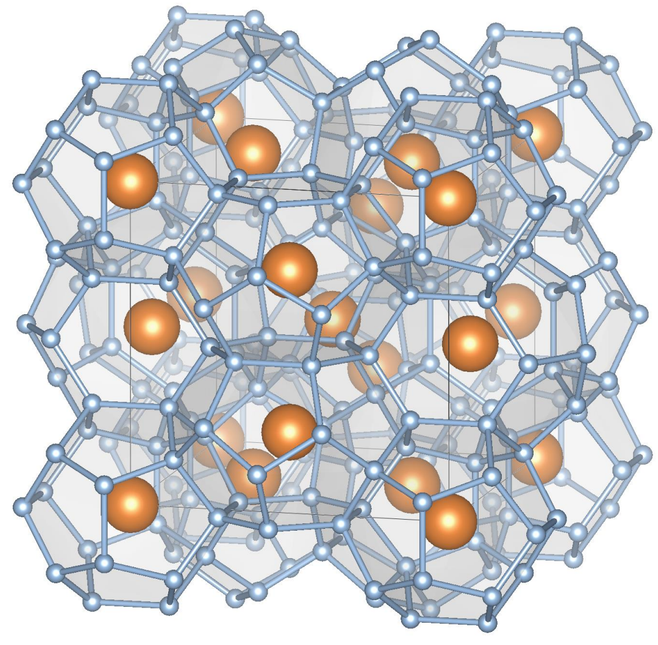

Complex unit cell

b. Spectral engineering for lower-k

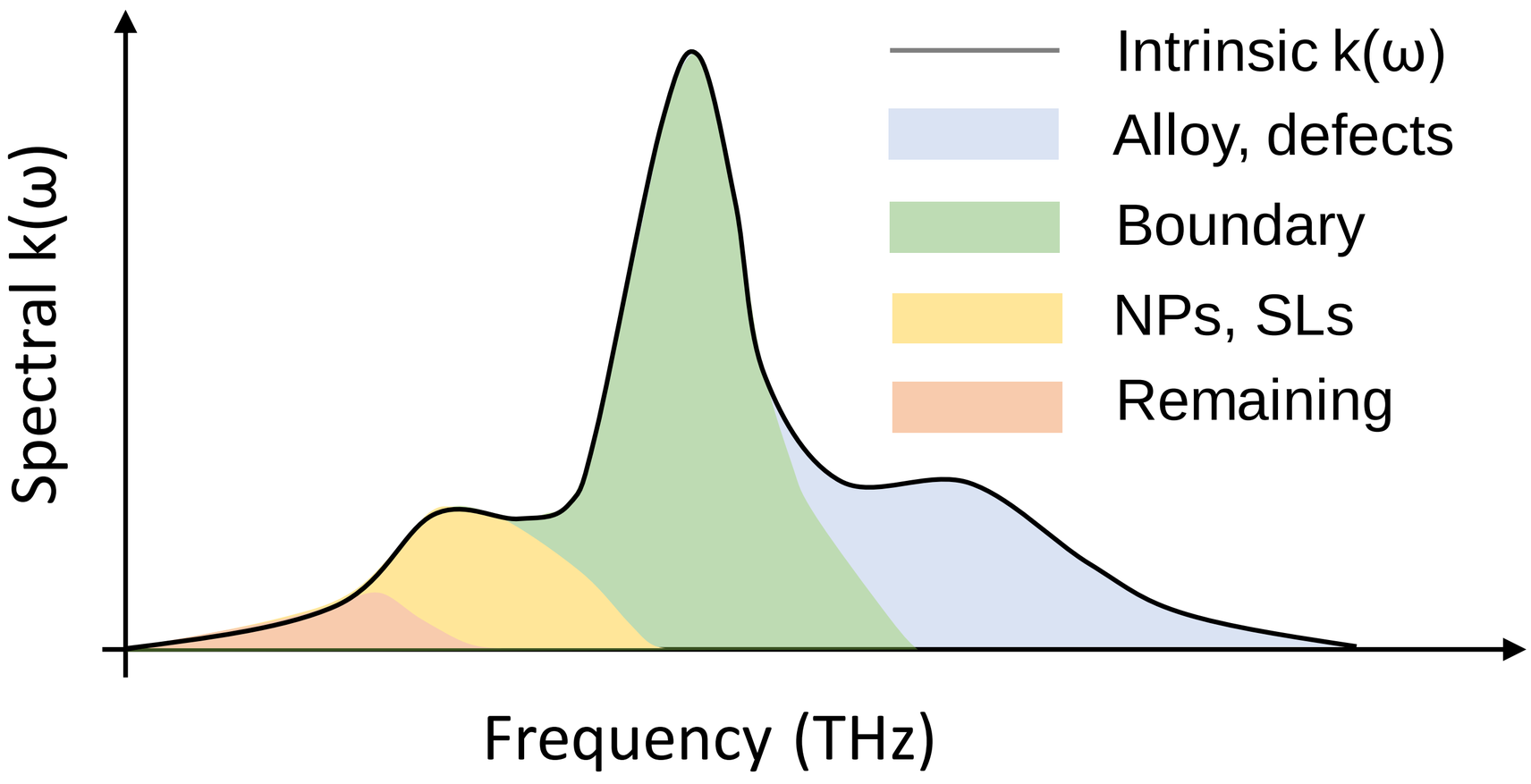

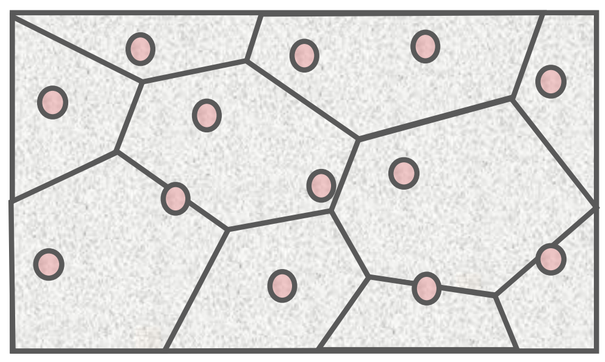

NP in alloyed NC

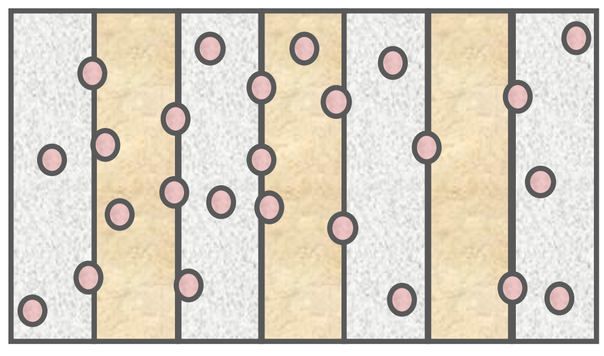

NP in alloyed SL

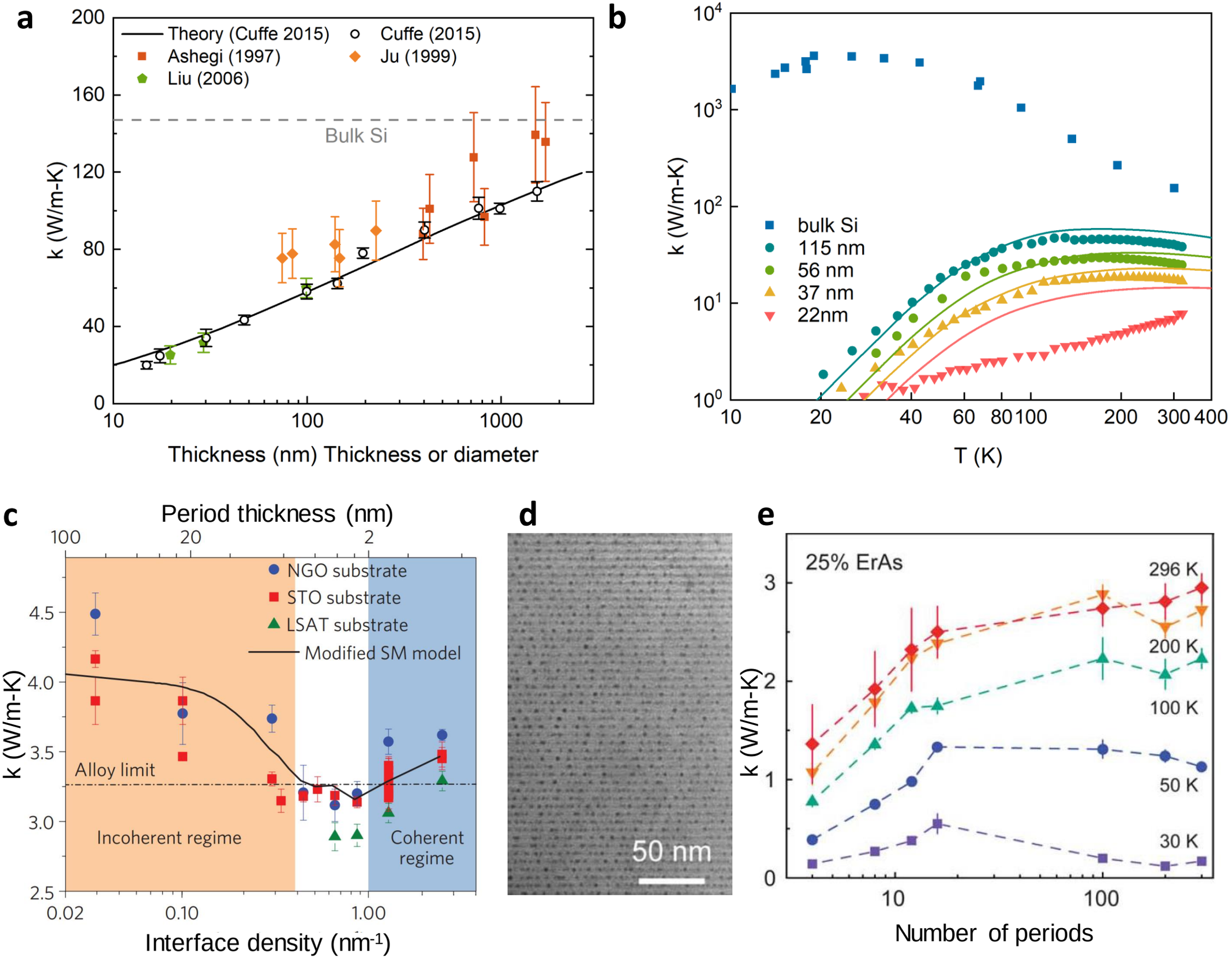
a
Theory (Cuffe 2015)
Cuffe (2015)
Ashegi (1997)
Ju (1999)
Liu (2006)
Bulk Si
k (W/m-K)
Thickness (nm) Thickness or diameter
b
bulk Si
115 nm
56 nm
37 nm
22nm
k (W/m-K)
T (K)
c
Period thickness (nm)
NGO substrate
STO substrate
LSAT substrate
Modified SM model
Alloy limit
Incoherent regime
Coherent regime
k (W/m-K)
Interface density (nm-1)
d
50 nm
e
25% ErAs
296 K
200 K
100 K
50 K
30 K
k (W/m-K)
Number of periods

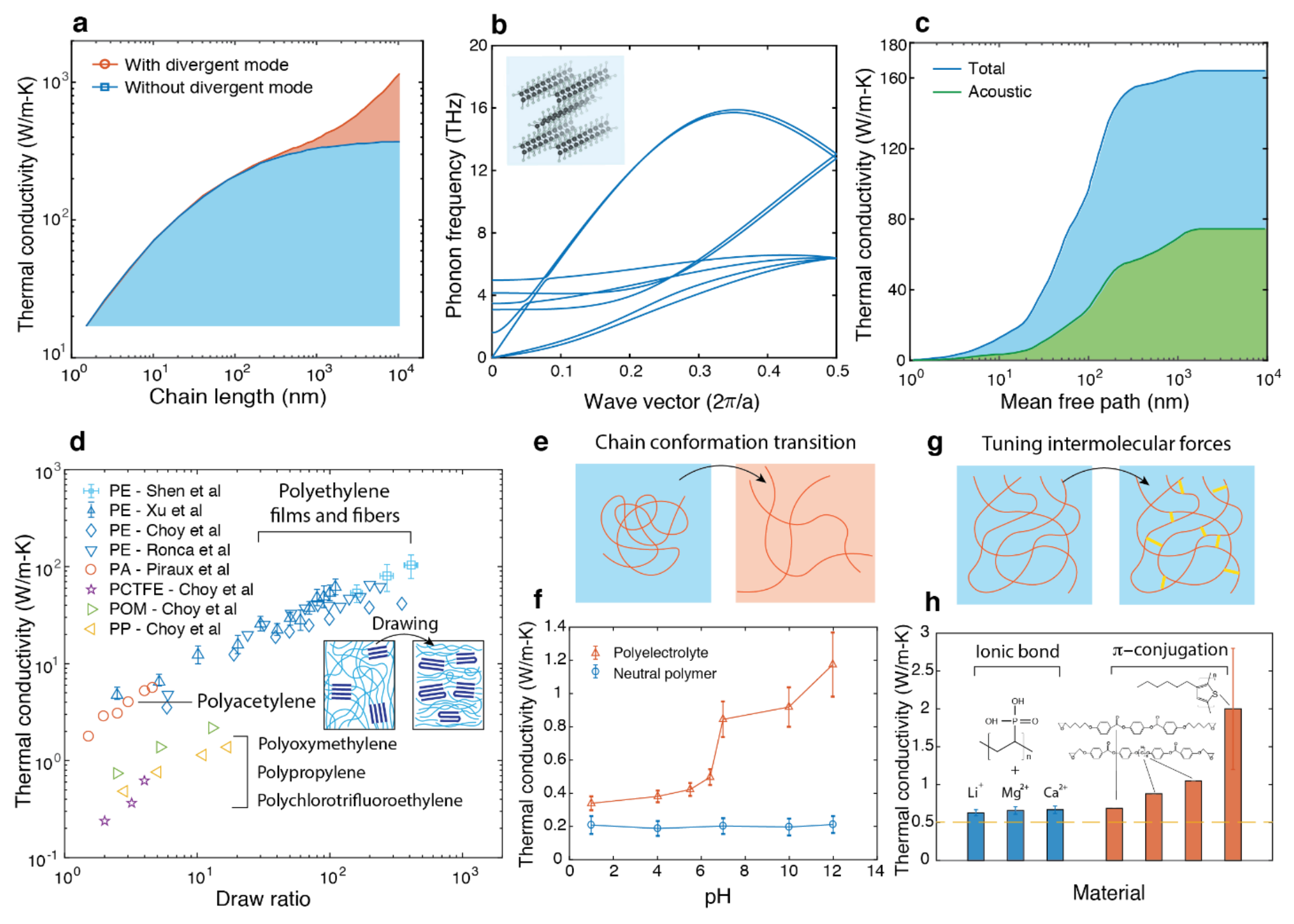
a
With divergent mode
Without divergent mode
Thermal conductivity (W/m-K)
Chain length (nm)
b
Phonon frequency (THz)
Wave vector (2π/a)
c
Total
Acoustic
Thermal conductivity (W/m-K)
Mean free path (nm)
d
PE - Shen et al
PE - Xu et al
PE - Choy et al
PE - Ronca et al
PA - Piraux et al
PCTFE - Choy et al
POM - Choy et al
PP - Choy et al
Polyethylene films and fibers
Drawing
Polyacetylene
Polyoxymethylene
Polypropylene
Polychlorotrifluoroethylene
Thermal conductivity (W/m-K)
Draw ratio
e
Chain conformation transition
g
Tuning intermolecular forces
f
Polyelectrolyte
Neutral polymer
Thermal conductivity (W/m-K)
pH
h
Ionic bond
π–conjugation
Li+
Mg2+
Ca2+
Thermal conductivity (W/m-K)
Material

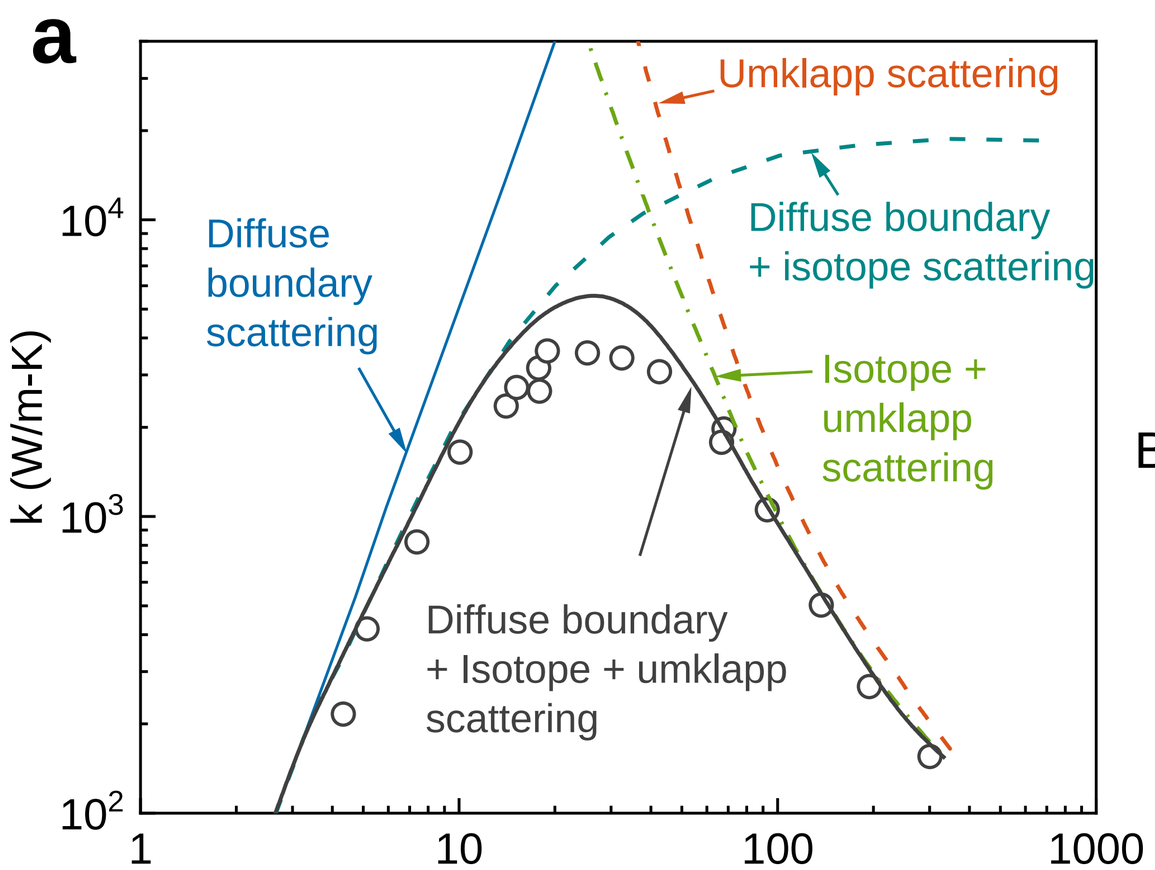
a
Umklapp scattering
Diffuse boundary + isotope scattering
Diffuse boundary scattering
Isotope + umklapp scattering
Diffuse boundary + Isotope + umklapp scattering
k (W/m-K)
10^4
10^3
10^2
1
10
100
1000

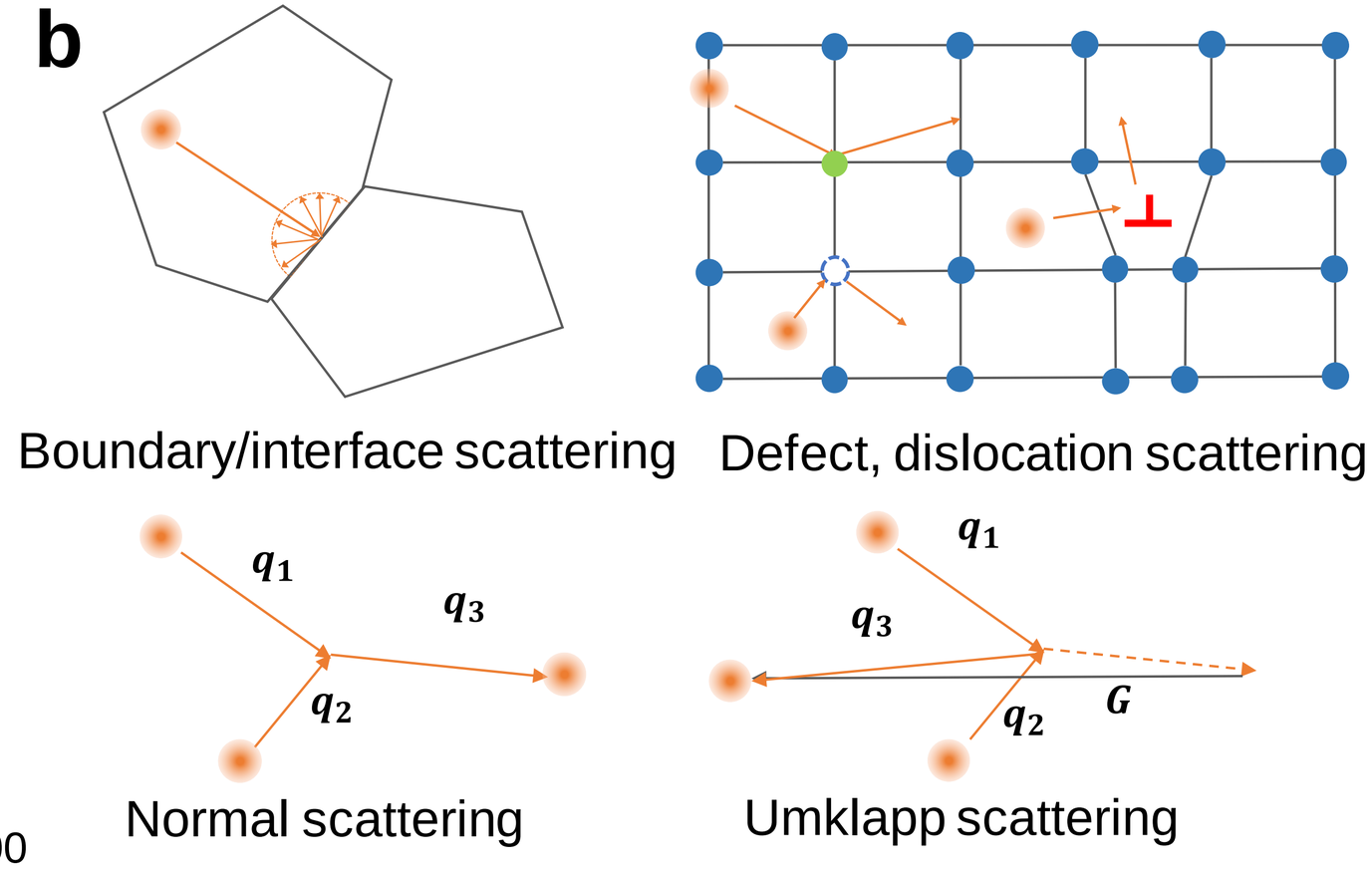
b
Boundary/interface scattering
Defect, dislocation scattering
q_1
q_3
q_2
Normal scattering
q_1
q_3
q_2
G
Umklapp scattering

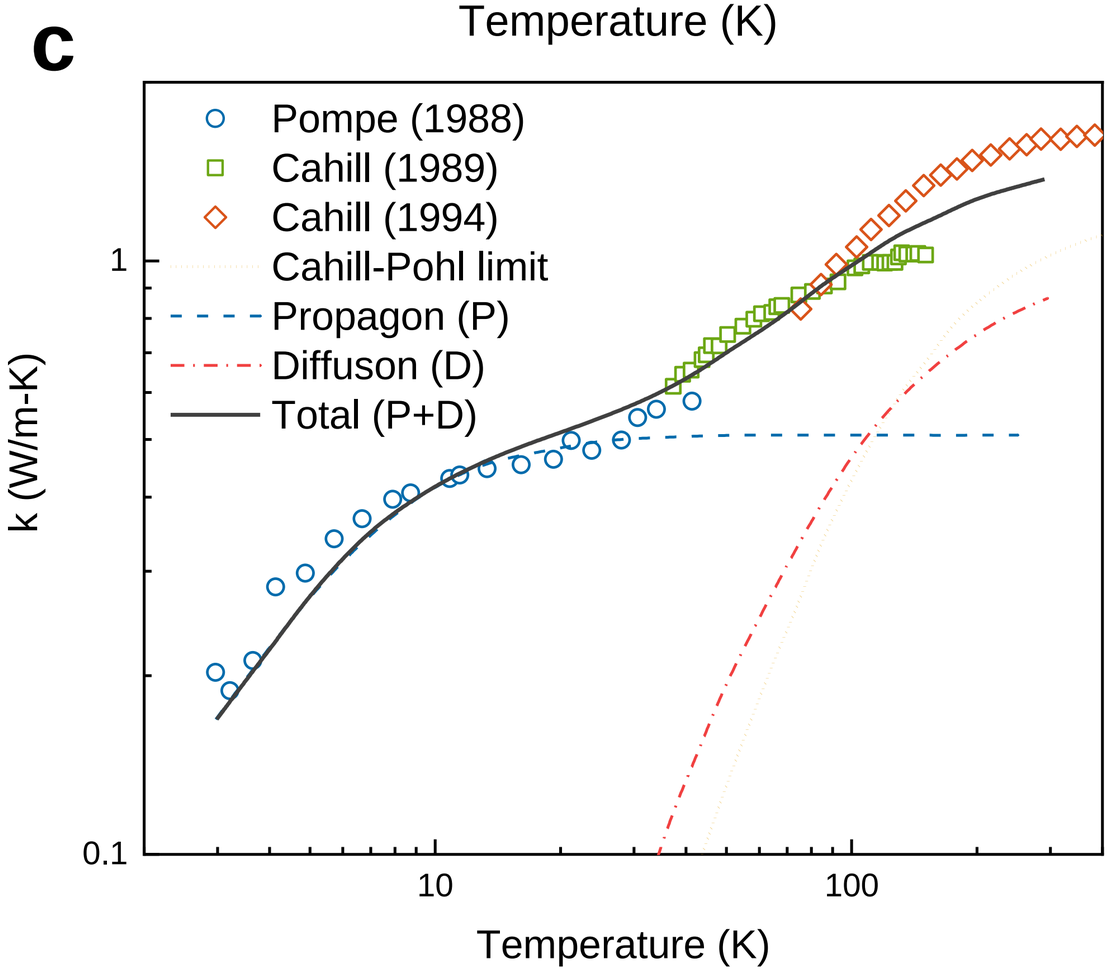
c
Temperature (K)
Pompe (1988)
Cahill (1989)
Cahill (1994)
Cahill-Pohl limit
Propagon (P)
Diffuson (D)
Total (P+D)
k (W/m-K)
1
0.1
10
100
Temperature (K)

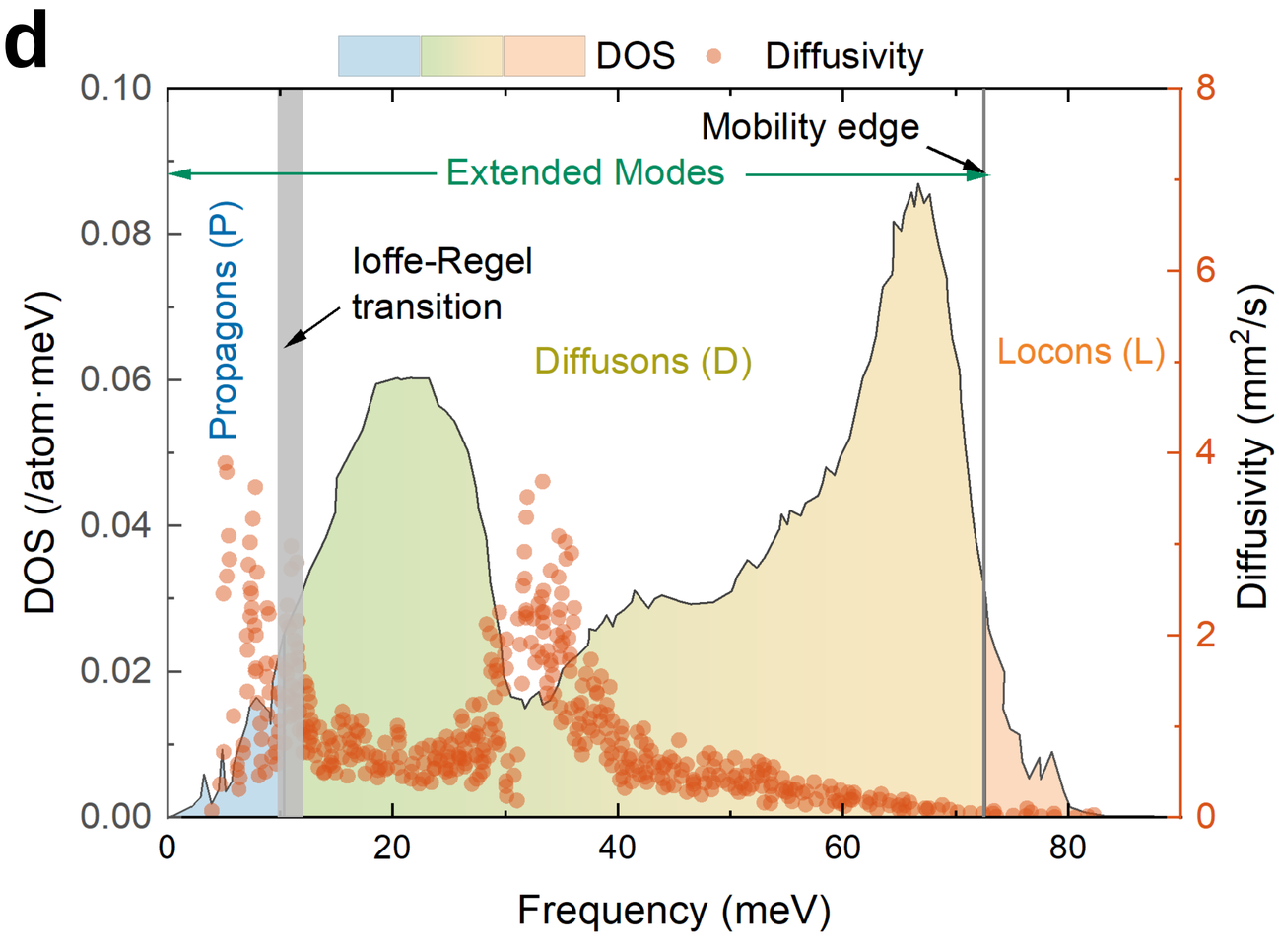
d
DOS
Diffusivity
Mobility edge
Extended Modes
Ioffe-Regel transition
Propagons (P)
Diffusons (D)
Locons (L)
DOS (/atom·meV)
Diffusivity (mm^2/s)
Frequency (meV)
0.10
0.08
0.06
0.04
0.02
0.00
8
6
4
2
0
0
20
40
60
80

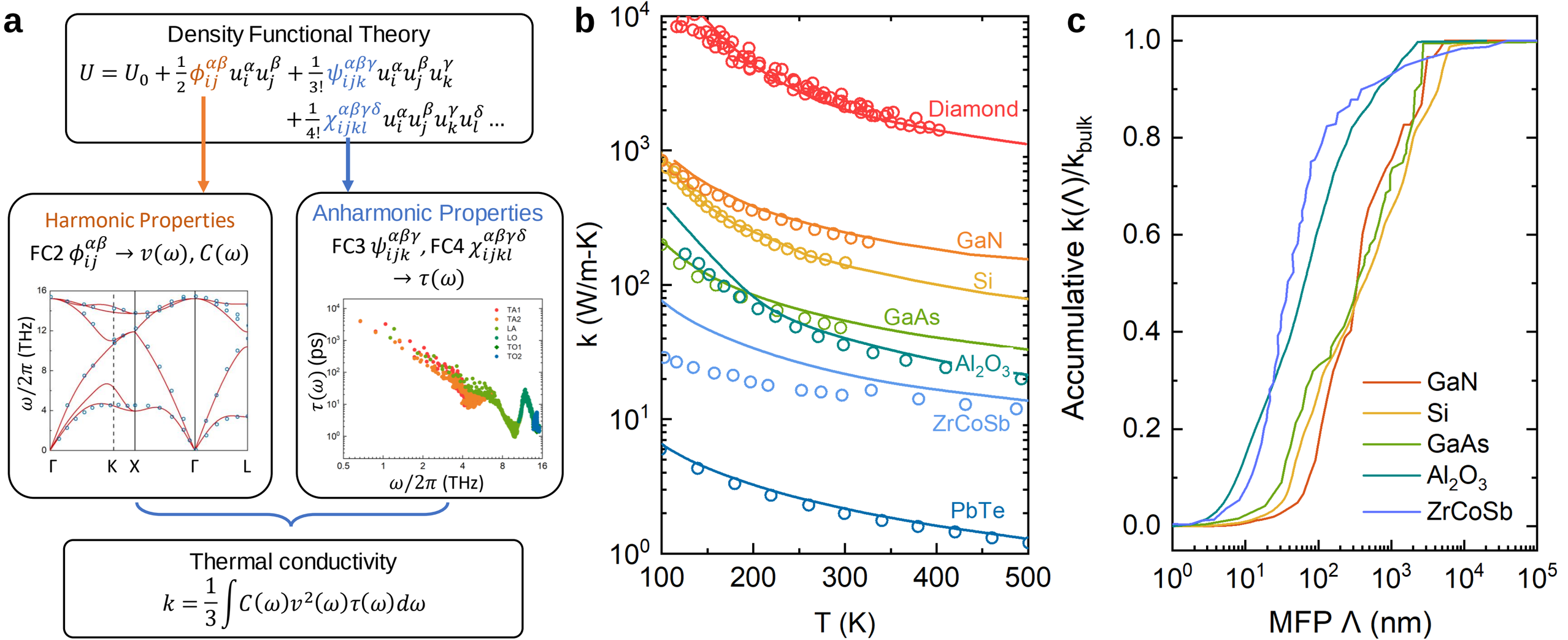
a
Density Functional Theory
$U = U_0 + \frac{1}{2}\phi_{ij}^{\alpha\beta} u_i^\alpha u_j^\beta + \frac{1}{3!}\psi_{ijk}^{\alpha\beta\gamma} u_i^\alpha u_j^\beta u_k^\gamma + \frac{1}{4!}\chi_{ijkl}^{\alpha\beta\gamma\delta} u_i^\alpha u_j^\beta u_k^\gamma u_l^\delta \ldots$
Harmonic Properties
FC2 $\phi_{ij}^{\alpha\beta} \rightarrow v(\omega), C(\omega)$
$\omega/2\pi$ (THz)
Γ K X Γ L
Anharmonic Properties
FC3 $\psi_{ijk}^{\alpha\beta\gamma}$, FC4 $\chi_{ijkl}^{\alpha\beta\gamma\delta}$
$\rightarrow \tau(\omega)$
TA1
TA2
LA
LO
TO1
TO2
$\tau(\omega)$ (ps)
$\omega/2\pi$ (THz)
Thermal conductivity
$k = \frac{1}{3}\int C(\omega) v^2(\omega) \tau(\omega) d\omega$
b
k (W/m-K)
T (K)
Diamond
GaN
Si
GaAs
Al_2O_3
ZrCoSb
PbTe
c
Accumulative $k(\Lambda)/k_{bulk}$
MFP Λ (nm)
GaN
Si
GaAs
Al_2O_3
ZrCoSb

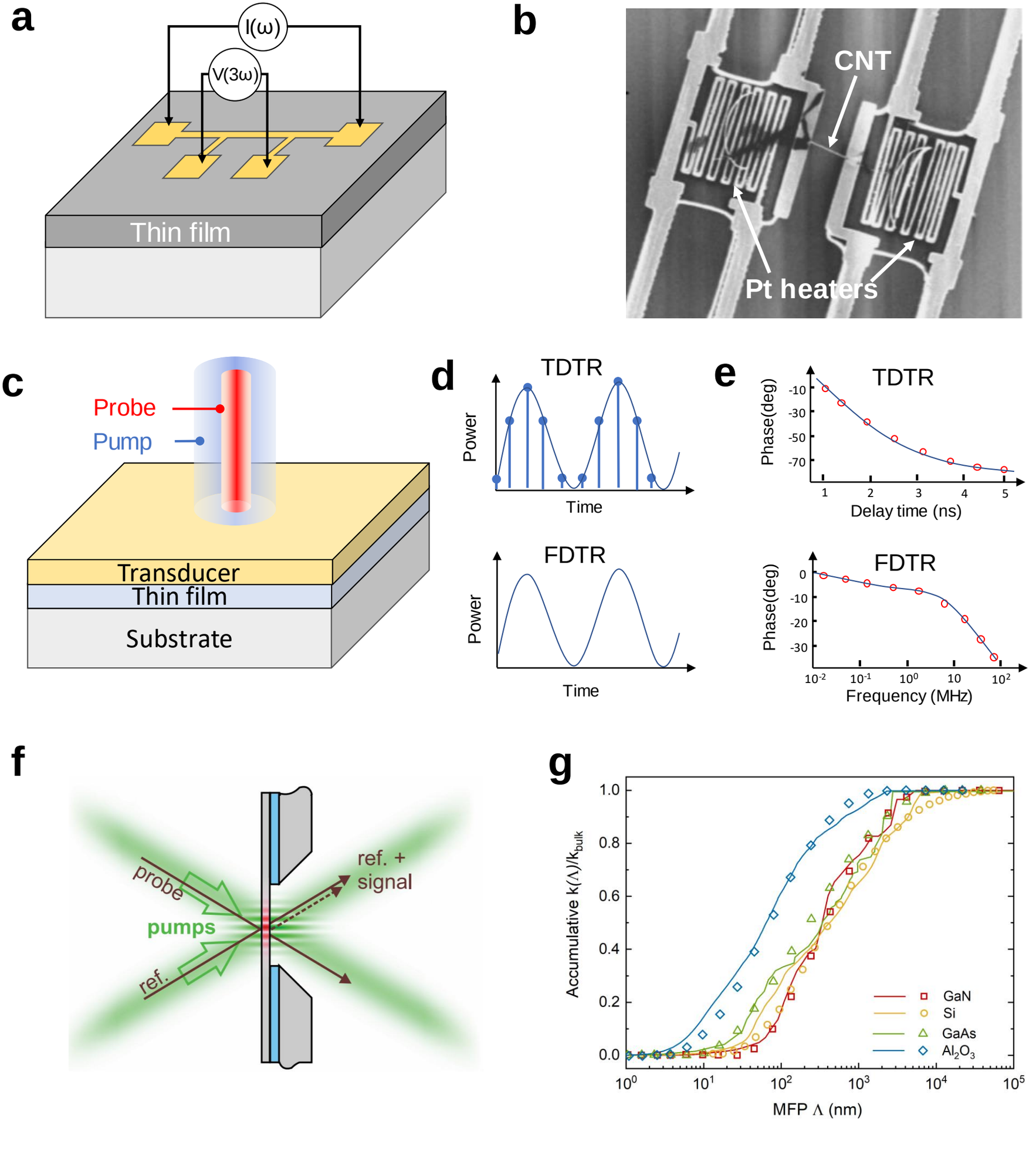
a
I(ω)
V(3ω)
Thin film
b
CNT
Pt heaters
c
Probe
Pump
Transducer
Thin film
Substrate
d
TDTR
Power
Time
FDTR
Power
Time
e
TDTR
Phase(deg)
-10
-30
-50
-70
1
2
3
4
5
Delay time (ns)
FDTR
Phase(deg)
0
-10
-20
-30
10-2
10-1
100
10
102
Frequency (MHz)
f
probe
pumps
ref.
ref. +
signal
g
Accumulative k(Λ)/kbulk
1.0
0.8
0.6
0.4
0.2
0.0
10^0
10^1
10^2
10^3
10^4
10^5
MFP Λ (nm)
GaN
Si
GaAs
Al2O3